Nuclear structure study of semi-magic ^{125}Sn via (n,γ) and (d,p) reactions

I. Tomandl and J. Honzátko
Nuclear Physics Institute, CZ-25068 Řež, Czech Republic

T. von Egidy, H.-F. Wirth, and T. Faestermann
Physik-Department, Technische Universität München, D-85748 Garching, Germany

V. Yu. Ponomarev
Institut für Kernphysik, Technische Universität Darmstadt, D-64289 Darmstadt, Germany

S. Pašić
Department of Physics, Faculty of Science, University of Zagreb, HR-10001 Zagreb, Croatia

R. Hertenberger, Y. Eisermann, and G. Graw
Department für Physik, Ludwig-Maximilians-Universität München, D-85748 Garching, Germany
(Received 12 August 2009; revised manuscript received 12 January 2011; published 29 April 2011)

The nuclear structure of the semi-magic isotope ^{125}Sn was investigated by means of the ^{124}Sn$(n_{\rm th},\gamma\gamma)^{125}$Sn reaction and the ^{124}Sn$(\vec{d},p)^{125}$Sn reaction. More than 400 levels, in most cases with their spin, parity, (d,p) spectroscopic factor, and γ decay, were identified. About 750 γ transitions from our $(n,\gamma\gamma)$ experiment form the essentially complete γ-decay scheme following thermal neutron capture. Using this extensive γ-decay scheme the neutron binding energy was determined to be 5733.5(2) keV. The strong correlation of the (d,p) strengths and the (n,γ) intensities for more than 50 levels gives evidence for the direct neutron capture process, which was studied in detail. The experimental data were compared with predictions of the quasiparticle phonon model.

DOI: 10.1103/PhysRevC.83.044326 PACS number(s): 21.10.Jx, 21.60.Ev, 25.40.Lw, 27.60.+j

I. INTRODUCTION

In our recent studies we have investigated the evolution of the nuclear structure of the long chain of the odd-A tellurium isotopes from ^{119}Te to ^{131}Te [1–7]. The continuation of this systematic investigation was one of the motivations for this work. Similar to the tellurium isotopes, several interesting effects might be observed in the neighboring odd-A tin isotopes. The dominant role of the direct capture mechanism can be assumed in thermal neutron capture of tin isotopes because of the very small cross sections. The odd tin isotopes enable us to disclose the almost complete distribution of the strength of the $3p_{3/2}$, $3p_{1/2}$, $2f_{7/2}$, and $2f_{5/2}$ neutron subshells. The microscopic study of the feeding of the $h_{11/2}$ isomer could explain the difference between the isomeric ratios for the tellurium and tin isotopes. Another motivation for our study of ^{125}Sn follows from the closed proton shell $Z = 50$ for the tin isotopes. Thus the odd tin isotopes are a good laboratory for testing the quasiparticle phonon model (QPM) in this mass region.

The mutually complementary methods, thermal radiative neutron capture and particle induced reactions, proved to be a powerful tool for nuclear structure studies. To investigate in detail ^{125}Sn we have combined results from the $(n_{\rm th},\gamma)$ measurement performed in Řež near Prague and the (d,p) measurement with the polarized beam of deuterons at Garching near Munich. The previous thermal neutron capture [8] and (d,p) [9] measurements do not provide sufficient spectroscopic data. Due to the extremely low thermal neutron cross section, 0.134 mb [10], the short paper on the $(n_{\rm th},\gamma)$ reaction [8] reported a very limited number of levels and γ transitions. The 30-keV energy resolution did not allow us to obtain a complete level scheme even below 2 MeV from the previous (d,p) experiment [9]. The results from the highly sensitive experimental setup in Řež [11] and the high-resolution Q3D magnetic spectrograph [12] will supersede data from these previous experiments. Besides these two reactions the present Nuclear Data Sheets (NDS) level and decay schemes of ^{125}Sn [13] are based on the data from the resonance neutron capture [14], the $(\alpha,^3{\rm He})$ reaction [9,15], the $(d,p\gamma)$ reaction [16], and the β decay [17].

Our experiments together with the methods of data evaluation are described in Sec. II. The construction of level and decay schemes and their discussions are presented in Sec. III. In this section the new value for the binding energy of neutron as well as the newly fitted parameters for the two-level density models, the constant temperature formula (CTF) and the back-shifted Fermi gas (BSFG), are given. The nuclear structure of ^{125}Sn is discussed in the framework of the quasiparticle phonon model (QPM) model. Its description and the comparison between experimental and theoretical results is written up in Sec. IV. The tin isotopes lie in a region where the presence of the direct capture mechanism in thermal neutron capture could be assumed. The role of this mechanism in the ^{124}Sn $(n_{\rm th},\gamma)$ reaction is investigated in detail in Sec. V.

II. EXPERIMENTS AND EVALUATION

A. Thermal neutron capture

The single ^{124}Sn(n,γ) and $\gamma\gamma$-coincidence spectra were measured with the facility installed at the LVR-15 reactor in Řež [11]. The spectra were taken with the two HPGe detectors with relative efficiencies of 25% and 28% and with the energy resolution of 1.9 keV at 1332 keV and 4.8 keV at 6 MeV for both detectors. The two HPGe crystals are positioned collaterally with the distance between the axes of the detectors of about 10 cm. The target of about 3.0 g with the enrichment of 97.9% in ^{124}Sn was inserted into a ^{6}Li-target holder. This holder was placed between the detectors. In this position, the three metallic target pellets each of 10 mm diameter were irradiated with a thermal neutron beam of about 10^6 n cm^{-2} s^{-1} from the external mirror neutron guide. The experimental arrangement has been described in detail elsewhere [11].

The single spectrum was taken with the 25% HPGe detector. The ten-day measurement was divided into 23 separate runs to obtain simultaneously the best statistics and the best energy resolution of the final single γ-ray spectrum. The close doublets in the low-energy spectrum of the ^{125}Sn decay were checked with a separate run covering the γ-ray spectrum within the energy interval up to 2200 keV. The energy calibration of the one-crystal spectra was performed with 38 well-known prominent background lines of Ge(n,γ) [18], ^{1}H(n,γ) [19], ^{35}Cl(n,γ) [20], ^{56}Fe(n,γ) [21], and ^{60}Co [22]. The relative efficiency of the HPGe detector was determined by means of intensities from the reaction ^{35}Cl(n,γ) [23], and from the decay of ^{152}Eu [24].

The isotope ^{125}Sn is unstable. The ground state and the first excited state at 27.5 keV decay via β^- decay with the half-life of 9.64 days and 9.52 min, respectively [24]. The strongest activation line from the decay of the isomeric state, 332 keV, was well observed in the single γ-ray spectrum. Taking into account the population ratio of the ground state and the isomeric state and the absolute intensity of this line per 100 decays, and assuming an equilibrium during irradiation of the ^{124}Sn target, we converted the relative intensities of γ rays into absolute intensities, the number of emitted γ rays per 100 captured thermal neutrons. The total systematic error following from this normalization procedure was estimated to be 5%. With respect to many unresolved doublets only the intensities of the strongest γ lines, about 80, were evaluated from the single γ-ray spectrum. Remaining intensities were calculated by means of the lines in the coincidence spectra. For these lines an γ-γ angular correlation was taken into account. For cascades with known spin sequences the intensities were corrected for the angular correlation. Otherwise, possible uncertainties associated with angular correlation were included into the final error.

To suppress cross talk between detectors in the coincidence measurements two lead plates of 2 mm thickness were inserted in the paths of γ rays from the target to the detectors. The coincidence data were accumulated in an event-by-event mode and were evaluated offline. The total run time of this experiment was ≈1730 h. From the large amount of coincidence data 565 coincidence spectra were generated. An example of a coincidence spectrum is shown in Fig. 1. The complete list of γ-ray energies observed in the single spectrum and in the γ-γ coincidence spectra is published in electronic form [25].

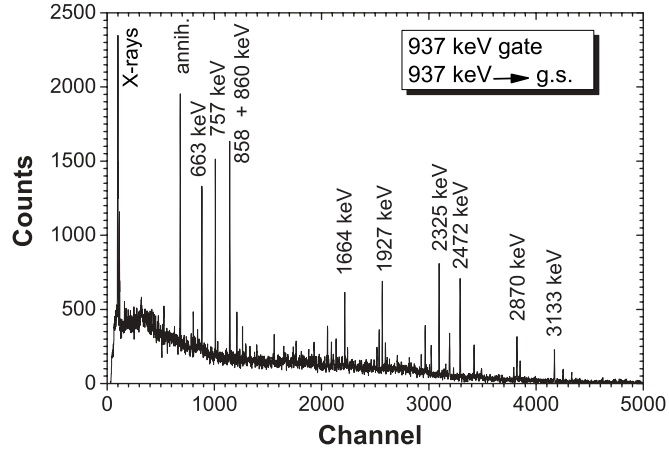

FIG. 1. The $\gamma\gamma$ coincidence spectrum of the 937-keV gate. The peaks are labeled with corresponding γ energies.

B. The (d,p) reaction with polarized beam

1. Experiment

The ^{124}Sn$(d,p)^{125}$Sn measurements were performed at the Tandem Accelerator of the Ludwig Maximilians University (LMU) and the Technical University of Munich (TUM). The amount of 143-μg/cm^2 metallic tin enriched in ^{124}Sn to 96.7% was evaporated on a carbon foil backing (about 4 μg/cm^2) and used as the target for this experiment. This target was irradiated by the 22-MeV polarized deuteron beam [26] with a vector polarization of ±70%. The beam intensity was about 500 nA. The outgoing protons were analyzed with the Q3D magnetic spectrograph [12] and detected with the 90-cm-long focal plane detector with cathode-strip readout [27]. The detector provided an excellent energy resolution of about 4 keV as well as a perfect background suppression using particle identification by means of combination of the energy-loss signal and the residual energy signal. The energy range covered by this detector was about 2 MeV. The acceptance opening of the magnetic spectrograph was 6 msr (slit of ±10 mm horizontally and ±20 mm vertically). Three different magnetic settings were adjusted to measure the proton spectra up to the excitation energy of 5.3 MeV. The proton spectra were taken at eight angles between 10° and 45° for both polarizations (spin up and spin down). The typical measurement time for each spectrum was about 30 min. An example of a proton spectrum is shown in Fig. 2. We evaluated the spectra with the computer code GASPAN [28].

Despite the high isotopic enrichment we observed several background lines in the proton spectra. Most of them originate from a (d,p) reaction on other tin isotopes. Fortunately, these background lines can be easily identified by means of the shift of the peak position at various scattering angles. To be sure that no spurious line will be interpreted as a new level the positions of the strongest lines from neighboring tin isotopes

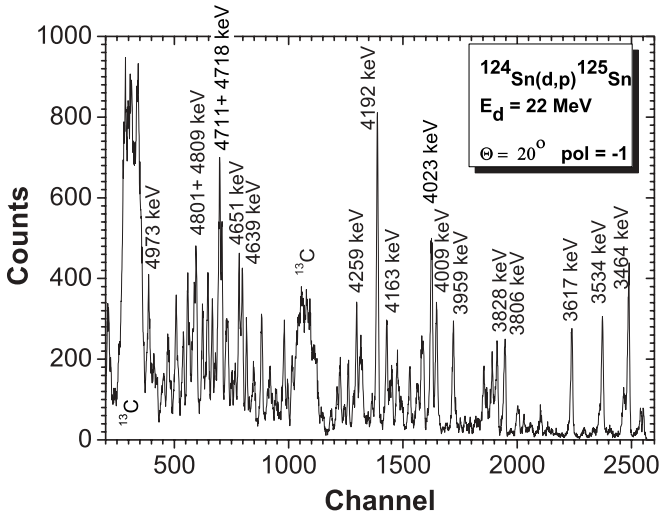

FIG. 2. A part of the proton spectrum from the ^{124}Sn$(d,p)^{125}$Sn reaction measured at $E_d = 22$ MeV and scattering angle $\Theta_{lab} = 20^\circ$. The peaks are labeled with the level excitation energy.

was checked using known kinematics. Broad background lines in the spectra were caused by the (d,p) reaction on light elements, mainly on ^{12}C (of backing) and oxygen.

The level energies evaluated from our (n,γ) experiment were used for the energy calibration of the proton spectra. In this calibration procedure the direct capture mechanism of the ^{124}Sn$(d,p)^{125}$Sn reaction (see Sec. V) plays an important role. Thanks to the correlation between (d,p) and (n,γ) strengths many levels populated with primary γ transitions could be associated with lines in the proton spectra. Thus these proton spectra were calibrated relatively precisely up to 5.3 MeV. The final (d,p) level energies were evaluated as averages over all scattering angles and both polarizations. The systematic error from the calibration does not exceed 0.3 keV in the region below 4.5 MeV. Above this, the lack of calibration points led to higher uncertainties. The systematic errors in the region above 4.5 MeV were linearly increased up to the value of 1.0 keV at the excitation energy of 5.3 MeV.

Absolute values of differential cross sections were normalized to the integrated beam current in a Faraday cup after the target. The total systematic error of differential cross sections was estimated to be less than 15%. Angular distributions of the experimental asymmetries were deduced from the equation

$$A_y = \frac{2}{3P_3}\frac{\sigma_+ - \sigma_-}{\sigma_+ + \sigma_-}, \quad (1)$$

where σ_+ and σ_- are the measured differential cross sections for two beam polarizations and $P_3 = 0.7$ is the vector polarization.

The summary of levels from the (d,p) experiment including level energies, differential cross sections at 20°, l transfers, spin and parity assignments, and spectroscopic strength is given in Table I. Complete experimental data from the (d,p) reaction can be found in the EXFOR database [29].

2. DWBA and CCBA analysis

The experimental differential cross sections were compared with the theoretical predictions from the distorted-wave Born approximation (DWBA) analysis performed with the computer program CHUCK3 [30]. The optical parameters were taken from the work by Strömich *et al.* [31]. These parameters are given in Table II.

In the DWBA analysis we assumed a direct reaction and a one-step stripping process. The spectroscopic factors S_{lj} were extracted from the relation

$$\frac{d\sigma^{\text{expt}}}{d\Omega} = S_{lj}\sigma_{lj}^{\text{CHUCK3}}, \quad (2)$$

where the experimental differential cross sections $\frac{d\sigma^{\text{expt}}}{d\Omega}$ are fitted with the theoretical DWBA single-particle cross sections $\sigma_{lj}^{\text{CHUCK3}}$. To obtain the spectroscopic factors we fitted the intensity of the first maxima of the theoretical distributions of the differential cross sections to the experimental ones. Fitted angular distributions up to 2 MeV are presented in Figs. 3–7.

It can be seen seen from Figs. 3–7 that in many cases the agreement between the DWBA calculation and the experimental data is not perfect. The question arises whether this agreement can be improved by inclusion of two-step processes in the calculation. To investigate and estimate the possible role of multistep processes the coupled-channel Born approximation (CCBA) analysis was performed for the $7/2^-$ level at 936 keV. This level was interpreted as the member of the $h_{11/2}$ family of states with the dominant contribution of the wave function $|2^+ \otimes 1h_{11/2}\rangle 7/2^-$. All three possible routes were taken into account in this CCBA calculation. For the collective excitation the adopted value of the deformation parameter $\beta_2 = 0.1$ from the compilation of $B(E2;2^+ \to 0^+)$ for the first 2^+ states [32] were used. The comparison of the one-step DWBA and CCBA calculation is shown in Fig. 4. Using CCBA calculation the slight improvement between calculated and experimental differential cross sections and asymmetries was achieved at higher scattering angles.

The big deviation between experimental and DWBA analyzing powers for the first two $l = 5$ states at 0 and 617 keV in Fig. 3 cannot be ascribed to the multistep process. However, the angular distribution of asymmetries for $11/2^-$ and $9/2^-$ states is extremely sensitive to optical-model parameters. The quite good agreement for these states can be obtained using slightly corrected optical-model parameters as, for instance, in our previous work [7]. Thus the experimental angular distribution of asymmetries for these two levels was utilized for the spin assignment of other $l = 5$ states.

Totally, we observed about 320 states in our (d,p) experiment. The high quality of the angular distributions of the differential cross sections and asymmetries enabled us to assign firmly unique spin and parity for most of these states. The mirrored asymmetries for states with spins of $J = l - 1/2$ and $J = l + 1/2$ additionally can help to assign l in cases of ambiguous angular distributions of the differential cross sections. Typically, one can avail the asymmetry distribution to distinguish between the $l = 2$ and $l = 3$ momentum transfers, which have very similar angular distributions of the differential cross sections.

TABLE I. Summary of levels observed in ^{124}Sn$(n,\gamma)^{125}$Sn and ^{124}Sn$(d,p)^{125}$Sn reaction. New spectroscopic data with respect to Ref. [13] are labeled by bold.

(n,γ)			(d,p)					Adopted	
Level energy (keV)	ΣI_γ (in)[a] per 100n	ΣI_γ (out)[a] per 100n	Level energy[b] (keV)	$\frac{d\sigma}{d\Omega}$ at 20° ($\frac{\mu b}{sr}$)	l	J^π	S_{dp} ($\times$100)	Level energy (keV)	J^π
0.0	2.8(6)		0.0	323(3)	5	$11/2^-$	27	0.0	$11/2^-$
27.7(1)	97.9(8)		27.6(1)	1717(7)	2	$3/2^+$	30	27.7(1)	$3/2^+$
215.2(1)	52.4(4)	52.4(6)	215.0(1)	277(3)	0	$1/2^+$	27	215.2(1)	$1/2^+$
617.9(1)	1.03(8)	1.15(1)	617.3(1)	3.4(4)	5	$9/2^-$	0.43	617.9(1)	$9/2^-$
854.9(1)	2.7(1)	3.0(3)	854.8(1)	22(1)	2	$5/2^+$	0.19	854.9(1)	**$5/2^+$**
930.4(1)	2.7(2)	2.55(2)	929.9(1)	23(2)	2	$3/2^+$	0.33	930.4(1)	**$3/2^+$**
936.5(1)	1.8(1)	1.7(6)	936.2(1)	108(3)	3	$7/2^-$	0.53[k]	936.5(1)	$7/2^-$
1059.5(1)	0.10(1)	0.27(2)	1059.6(2)	5.9(4)	(4)	$7/2^+$	0.010[k]	1059.5(1)	$7/2^+$
1072.0(1)	1.85(7)	2.23(4)	1072.2(1)	8.9(5)	(2)	$(3/2^+)$	0.17	1072.0(1)	**$3/2^+$**
			1087.7(1)	5.5(4)	(5)	$11/2^-$	0.25	**1087.7(3)**	**$11/2^-$**
1187.5(1)	2.85(8)	4.03(4)	1187.9(2)	2.4(3)	0	$1/2^+$	0.17	1187.5(1)	**$1/2^+$**
1250.1(1)	0.30(3)	0.45(7)	1250.7(2)	1.1(4)[e]	3	$7/2^-$	0.070	**1250.1(1)**	**$7/2^-$**
1259.2(1)	1.42(5)	1.50(4)	1259.3(1)	394(84)	2	$5/2^+$	3.9	1259.2(1)	$5/2^+$
1362.2(2)	0.009(3)	0.3(1)	1362.4(1)	62(1)	4	$7/2^+$	3.0	1362.2(2)	$7/2^+$
			1435.5(2)	2.0(4)	5	$(9/2^-)$	0.27	**1435.5(4)**	**$(9/2^-)$**
1538.7(1)	1.56(9)	1.80(4)	1538.7(1)	245(3)	2	$5/2^+$	2.2	1538.7(1)	$5/2^+$
1599.1(1)	0.25(2)	0.58(5)	1599.2(2)	2.6(4)	3	$5/2^-$	0.037	**1599.1(1)**	**$5/2^-$**
1683.6(1)	0.22(2)	0.35(5)						**1683.6(1)**	**$1/2^+$,$3/2$**
1693.5(1)	0.28(2)	0.39(2)	1692.6(2)	3.9(4)	(3,4)	$(5/2^-,7/2^+)$	(0.036, 0.13)	**1693.5(1)**	**$(5/2^-,7/2^+)$**
1746.6(2)?		0.04(1)						**1746.6(2)?**	**$(7/2^+)$**
1757.9(1)	0.37(5)	0.7(1)	1757.9(1)	2.6(4)	0	$1/2^+$	0.18	1757.9(1)	$1/2^+$
1794.3(1)	0.10(2)	0.54(5)						**1794.3(1)**	**$(3/2^-)$**
1796.4(1)	0.52(4)	0.9(1)	1796.2(1)	35(1)	2	$5/2^+$	0.32	**1796.4(1)**	**$5/2^+$**
1844.3(2)		0.10(1)	1843.3(4)	1.1(2)	(5)	$(11/2^-)$	0.054	**1844.3(2)**	**$(11/2^-)$**
1874.4(1)	0.20(2)	0.40(3)	1874.2(1)	11(1)	2	$5/2^+$	0.12	1874.4(1)	**$5/2^+$**
1884.1(1)	0.41(4)	0.9(1)	1883.7(2)	3.1(4)	1	$3/2^-$	0.080	**1884.1(1)**	**$3/2^-$**
1901.8(3)	0.02(1)	0.05(1)						**1901.8(3)**	**$5/2^-$,$7/2^-$**
			1936.7(3)	2.4(4)	(3)	$(7/2^-)$	0.019	**1936.7(4)**	**$(7/2^-)$**
1938.2(2)	0.15(2)	0.22(7)						**1938.2(2)**	**$1/2^+$,$3/2^+$**
1967.4(2)	0.16(2)	0.4(1)						**1967.4(2)**	**$1/2^+$,$3/2$,$5/2^+$**
1984.2(2)	0.04(1)	0.11(1)	1983.6(20)	0.75(24)[f]	(3)	$(7/2^-)$	0.006	**1984.2(2)**	**$(7/2^-)$**
			2018.9(2)	2.7(5)	(4)	$(7/2^+)$	0.10	**2018.9(4)**	**$(7/2^+)$**
			2065.5(3)	1.7(3)	3	$7/2^-$	0.011	**2065.5(4)**	**$7/2^-$**
			2099.0(3)	1.7(4)	2	$5/2^+$	0.021	**2099.0(4)**	**$5/2^+$**
2105.5(2)	0.02(1)	0.11(1)	2104.5(2)	2.7(4)	1	$3/2^-$	0.038	**2105.5(2)**	**$3/2^-$**
			2111.0(5)	1.8(4)	(2)	$(5/2^+,3/2^+)$	0.015	**2111.0(6)**	**$(5/2^+,3/2^+)$**
2181.1(1)	0.15(2)	0.14(2)						**2181.1(1)**	**$(5/2^+)$**
			2185.4(3)	1.3(3)	4	$7/2^+$	0.044	**2185.4(4)**	**$7/2^+$**
2186.7(1)	0.06(1)	0.31(3)						**2186.7(1)**	**$(5/2^+)$**
2196.8(3)	0.05(1)	0.02(1)	2196.3(3)	1.8(3)	2	$3/2^+$	0.020	**2196.8(3)**	**$3/2^+$**
2228.4(2)	0.01(1)	0.08(1)						**2228.4(2)**	**$1/2^+$,$3/2$,$5/2^-$**
2251.1(2)	0.02(1)	0.15(5)	2250.8(3)	2.4(4)	0	$1/2^+$	0.20	2251.1(2)	**$1/2^+$**
2258.5(3)?	0.03(1)	0.01(1)						**2258.5(3)?**	**$1/2$,$3/2$,$5/2^-$**
			2272.8(4)	0.93(27)	5	$9/2^-$	0.10	**2272.8(5)**	**$9/2^-$**
2284.9(2)	0.07(1)	0.09(2)	2285.5(2)	1.9(3)	(3)	$(5/2^-)$	0.020	2284.9(2)	**$5/2^-$**
2295.2(3)	0.01(1)	0.03(1)						**2295.2(3)?**	**$3/2^+$,$5/2$,$7/2^+$**
2333.7(2)	0.02(1)	0.07(1)						2333.7(2)	**$1/2$,$3/2$**
2347.8(1)	0.18(2)	0.50(5)	2347.6(1)	17(1)	1	$3/2^-$	0.18	2347.8(1)	**$3/2^-$**
			2378.2(2)	39(1)	3	$7/2^-$	0.18	**2378.2(4)**	**$7/2^-$**
			2383.3(5)	4(3)[g]	(3)	$(7/2^-)$	0.036	**2383.3(6)**	**$(7/2^-)$**
2385.5(3)?		0.05(1)						**2385.5(3)?**	**$1/2^+$,$3/2$,$5/2^+$**
			2393.4(1)	12(1)	2	$3/2^+$	0.083	**2393.4(3)**	**$3/2^+$**
2397.6(3)	0.07(5)	0.06(1)						**2397.6(3)**	**$1/2^+$,$3/2$,$5/2^+$**
			2413.7(2)	6.7(6)	(3)	$(7/2^-)$	0.036	**2413.7(4)**	**$(7/2^-)$**

TABLE I. (*Continued.*)

(n,γ)			(d,p)					Adopted	
Level energy (keV)	ΣI_γ (in)[a] per 100n	ΣI_γ (out)[a] per 100n	Level energy[b] (keV)	$\frac{d\sigma}{d\Omega}$ at 20° ($\frac{\mu b}{sr}$)	l	J^π	S_{dp} ($\times$100)	Level energy (keV)	J^π
2420.9(2)	0.05(1)	0.08(2)						2420.9(2)	$(5/2^-)$
2441.6(2)		0.10(2)						2441.6(2)	
2446.4(2)		0.06(2)	2445.9(3)	2.9(5)	3	$7/2^-$	0.014	2446.4(2)	$7/2^-$
			2452.7(3)	5.9(11)	(3)	$(7/2^-)$	0.030	2452.7(4)	$(7/2^-)$
			2459.5(1)	31(1)	3	$7/2^-$	0.15	2459.5(3)	$7/2^-$
			2473.0(2)	9.2(10)	(2)	$(5/2^+)$	0.032	2473.0(4)	$(5/2^+)$
			2482.6(3)	8.5(10)	2	$3/2^+$	0.037	2482.6(4)	$3/2^+$
			2499.0(3)	4.5(6)	4	$7/2^+$	0.11	2499.0(4)	$7/2^+$
			2517.8(1)	30(1)	3	$7/2^-$	0.14	2517.8(3)	$7/2^-$
2520.8(2)?	0.01(1)	0.04(2)						2520.8(2)?	
			2521.7(3)	3.4(7)[e]	(3)	$(7/2^-)$	0.050	2521.7(4)	$(7/2^-)$
2529.2(2)	0.05(1)	0.10(1)	2530.0(3)	3.6(5)[e]	1	$1/2^-$	0.11	2529.2(2)	$1/2^-$
			2541.6(1)	9.4(6)	3	$7/2^-$	0.047	2541.6(3)	$7/2^-$
2561.3(2)	0.22(2)	0.20(4)	2561.3(2)	4.9(5)	1	$3/2^-$	0.080	2561.3(2)	$3/2^-$
			2574.4(4)	0.63(37)[e]	(3)	$(7/2^-)$	0.027	2574.4(5)	$(7/2^-)$
2582.6(2)	0.10(6)	0.17(3)						2582.6(2)	$(3/2^-)$
			2583.6(1)	48(3)	3	$7/2^-$	0.24	2583.6(3)	$7/2^-$
			2595.2(2)	5.6(9)	3	$7/2^-$	0.036	2595.2(4)	$7/2^-$
			2603.6(3)	3.4(6)	4	$7/2^+$	0.10	2603.6(4)	$7/2^+$
			2614.0(1)	15(2)	3	$7/2^-$	0.072	2614.0(3)	$7/2^-$
			2619.8(4)	6.7(14)	(3)	$(7/2^-)$	0.036	2619.8(5)	$(7/2^-)$
			2628.9(4)	3.0(7)	5	$9/2^-$	0.17	2628.9(5)	$9/2^-$
			2636.7(4)	2.7(7)	(3)	$(7/2^-)$	0.014	2636.7(5)	$(7/2^-)$
2646.6(3)	0.01(1)	0.02(1)	2646.5(3)	3.6(7)	(1)	$(3/2^-)$	0.028	2646.6(3)	$(3/2^-)$
			2657.0(2)	4.2(6)	1	$3/2^-$	0.038	2657.0(4)	$3/2^-$
			2663.3(3)	1.7(5)[e]	(5)	$(9/2^-)$	0.12	2663.3(4)	$(9/2^-)$
			2674.5(2)	6.6(7)	3	$7/2^-$	0.032	2674.5(4)	$7/2^-$
			2683.6(4)	1.4(4)[e]	5	$9/2^-$	0.11	2683.6(5)	$9/2^-$
			2696.6(4)	0.93(40)	0	$1/2^+$	0.074	2696.6(5)	$1/2^+$
2703.5(3)	0.01(1)	0.04(1)						2703.5(3)	$(5/2^+)$
			2705.1(3)	2.4(5)	(3)	$(7/2^-)$	0.012	2705.1(4)	$(7/2^-)$
			2715.2(1)	16(1)	3	$7/2^-$	0.077	2715.2(3)	$7/2^-$
			2722.0(2)	2.9(6)	5	$9/2^-$	0.29	2722.0(4)	$9/2^-$
			2730.5(2)	2.8(6)[e]	(3)	$(7/2^-)$	0.032	2730.5(4)	$(7/2^-)$
			2736.7(2)?	2.3(6)[f]				2736.7(4)?	
			2754.8(1)	6228(28)	3	$7/2^-$	30	2754.8(3)	$7/2^-$
2770.5(2)	0.05(1)	0.12(6)						2770.5(2)	$1/2,3/2,5/2^+$
			2797.9(1)	558(9)	3	$7/2^-$	2.7	2797.9(3)	$7/2^-$
2824.7(4)?		0.08(2)						2824.7(4)?	
			2843.8(2)	8.3(14)	2	$3/2^+$	0.091	2843.8(4)	$3/2^+$
			2855.0(5)	7.9(12)	(2)	$(5/2^+)$	0.068	2855.0(6)	$(5/2^+)$
			2873.3(1)	238(3)	3	$7/2^-$	1.2	2873.3(3)	$7/2^-$
2885.5(1)	0.21(6)	0.69(5)	2885.8(2)	12(1)	1	$3/2^-$	0.17	2885.5(1)	$3/2^-$
			2893.9(2)	7.2(14)	3	$7/2^-$	0.034	2893.9(4)	$7/2^-$
2897.5(3)?		0.05(1)						2897.5(3)?	
			2915.6(1)	17(1)	3	$7/2^-$	0.081	2915.6(3)	$7/2^-$
			2932.6(2)	5.5(8)	3	$7/2^-$	0.034	2932.6(3)	$7/2^-$
			2943.6(3)	2.3(5)[e]	3	$7/2^-$	0.023	2943.6(4)	$7/2^-$
			2956.5(5)	1.3(5)[e]	(1)	$(3/2^-)$	0.023	2956.5(6)	$(3/2^-)$
			2969.5(3)	1.9(5)	(1)	$(3/2^-)$	0.028	2969.5(4)	$(3/2^-)$
			2989.3(1)	223(3)	3	$7/2^-$	1.1	2989.3(3)	$7/2^-$
			3017.1(1)	221(2)	3	$7/2^-$	1.0	3017.1(3)	$7/2^-$
			3044.9(4)	2.3(5)[g]	(1)	$(3/2^-)$	0.019	3044.9(5)	$(3/2^-)$
			3056.9(1)	134(2)	3	$7/2^-$	0.63	3056.9(3)	$7/2^-$
			3076.5(1)	215(2)	3	$7/2^-$	1.0	3076.5(3)	$7/2^-$

TABLE I. (*Continued.*)

(n,γ)			(d,p)					Adopted	
Level energy (keV)	ΣI_γ (in)[a] per 100n	ΣI_γ (out)[a] per 100n	Level energy[b] (keV)	$\frac{d\sigma}{d\Omega}$ at 20° ($\frac{\mu b}{sr}$)	l	J^π	S_{dp} ($\times$100)	Level energy (keV)	J^π
3077.4(2)	0.02(1)	0.13(1)						3077.4(2)	1/2,3/2,5/2+
			3097.4(5)	1.1(5)[g]	(3)	$(7/2^-)$	0.013	3097.4(6)	$(7/2^-)$
			3105.3(1)	37(1)	3	$7/2^-$	0.17	3105.3(3)	$7/2^-$
			3141.2(1)	24(1)	3	$7/2^-$	0.11	3141.2(3)	$7/2^-$
			3159.0(1)	187(2)	3	$7/2^-$	0.86	3159.0(3)	$7/2^-$
3163.7(2)	0.20(6)	0.22(3)						3163.7(2)	$3/2^-$
			3175.1(1)	143(2)	3	$7/2^-$	0.68	3175.1(3)	$7/2^-$
			3190.3(1)	340(3)	3	$7/2^-$	1.5	3190.3(3)	$7/2^-$
			3213.2(2)	2.7(6)	1	$3/2^-$	0.047	3213.2(4)	$3/2^-$
3236.7(2)	0.43(2)	0.70(4)	3236.6(1)	14(4)	1	$3/2^-$	0.27	3236.7(2)	$3/2^-$
			3248.9(3)	1.0(5)	(1)	$(3/2^-)$	0.028	3248.9(4)	$(3/2^-)$
			3258.6(1)	16(1)	3	$7/2^-$	0.072	3258.6(3)	$7/2^-$
			3266.1(1)	13(1)	3	$7/2^-$	0.059	3266.1(3)	$7/2^-$
			3284.4(2)	2.9(4)	2	$3/2^+$	0.037	3284.4(4)	$3/2^+$
			3296.2(1)	6.4(5)	1	$3/2^-$	0.085	3296.2(3)	$3/2^-$
			3318.2(1)	13(7)	3	$7/2^-$	0.059	3318.2(3)	$7/2^-$
3336.1(1)	9.7(1)	10.3(1)	3336.1(1)	330(3)	1	$3/2^-$	5.7	3336.1(1)	$3/2^-$
			3354.7(1)	27(1)	3	$7/2^-$	0.13	3354.7(3)	$7/2^-$
3362.3(1)	1.31(2)	1.44(5)	3362.2(1)	54(1)	1	$3/2^-$	0.85	3362.3(1)	$3/2^-$
			3383.3(1)	52(1)	3	$7/2^-$	0.23	3383.3(3)	$7/2^-$
3408.7(1)	27.9(2)	30.3(1)	3408.5(1)	1041(6)	1	$3/2^-$	18	3408.7(1)	$3/2^-$
			3425.6(2)	9.5(14)	1	$3/2^-$	0.13	3425.6(4)	$3/2^-$
			3432.8(1)	16(1)	3	$7/2^-$	0.072	3432.8(3)	$7/2^-$
			3440.7(3)	3.2(8)	1	$3/2^-$	0.047	3440.7(4)	$3/2^-$
			3448.2(2)	4.0(6)	1	$3/2^-$	0.066	3448.2(4)	$3/2^-$
3463.7(1)	4.2(1)	3.6(1)	3463.5(1)	163(2)	1	$3/2^-$	2.6	3463.7(1)	$3/2^-$
3476.2(2)	1.13(2)	1.0(2)	3476.1(1)	37(1)	1	$3/2^-$	0.57	3476.2(2)	$3/2^-$
			3482.9(3)	6.9(9)	1	$3/2^-$	0.11	3482.9(4)	$3/2^-$
			3495.2(3)	2.9(5)	1	$3/2^-$	0.047	3495.2(4)	$3/2^-$
			3504.1(1)	6.9(11)	1	$1/2^-$	0.12	3504.1(3)	$1/2^-$
3513.4(2)	0.43(22)	0.39(5)	3513.5(1)	16(1)	1	$1/2^-$	0.58	3513.4(2)	$1/2^-$
			3525.5(2)	11(1)	3	$7/2^-$	0.054	3525.5(4)	$7/2^-$
3533.6(1)	2.73(3)	2.97(5)	3533.8(1)	107(2)	1	$3/2^-$	1.7	3533.6(1)	$3/2^-$
			3542.3(1)	17(1)	3	$7/2^-$	0.081	3542.3(3)	$7/2^-$
			3550.9(4)	3.6(8)	(1)	$(3/2^-)$	0.068	3550.9(5)	$(3/2^-)$
3558.1(2)	0.14(10)	0.14(3)	3558.2(1)	9.2(7)	1	$3/2^-$	0.11	3558.1(2)	$3/2^-$
			3569.0(5)	1.4(6)				3569.0(6)	
3581.4(2)	0.15(3)	0.09(2)	3581.6(2)	6.5(11)	1	$3/2^-$	0.13	3581.4(2)	$3/2^-$
			3586.8(2)	6.7(12)	1	$3/2^-$	0.091	3586.8(4)	$3/2^-$
3617.1(1)	1.48(2)	1.22(15)	3617.3(1)	120(4)	1	$3/2^-$	1.7	3617.1(1)	$3/2^-$
			3628.8(3)	3.4(17)	1	$3/2^-$	0.057	3628.8(4)	$3/2^-$
			3643.5(5)	1.8(5)[f]				3643.5(6)	
			3647.3(5)	4.2(8)[h]	(3)	$(7/2^-)$	0.016	3647.3(6)	$(7/2^-)$
			3657.0(3)	4.8(7)	3	$7/2^-$	0.017	3657.0(4)	$7/2^-$
			3673.3(2)	7.9(9)	3	$5/2^-$	0.048	3673.3(4)	$5/2^-$
3684.5(3)		0.08(2)	3684.5(2)	7.8(14)	1	$3/2^-$	0.095	3684.5(3)	$3/2^-$
			3692.1(8)	2.3(8)	(1)	$(1/2^-,3/2^-)$	0.077	3692.1(8)	$(1/2^-,3/2^-)$
3702.5(3)	0.09(5)	0.08(2)	3703.6(1)	26(3)	1	$(3/2^-)$	0.38	3702.5(3)	$(3/2^-)$
			3710.5(3)	8.9(28)	3	$5/2^-$	0.060	3710.5(4)	$5/2^-$
			3727.0(2)	9.5(17)	(5)	$(9/2^-)$	0.34	3727.0(4)	$(9/2^-)$
			3731.2(2)	14(2)	3	$5/2^-$	0.11	3731.2(4)	$5/2^-$
3742.2(3)	0.02(1)	0.06(1)	3742.4(2)	6.7(11)	1	$3/2^-$	0.057	3742.2(3)	$3/2^-$
			3751.3(1)	17(1)	3	$7/2^-$	0.072	3751.3(3)	$7/2^-$
			3759.3(4)	3.1(6)	3	$7/2^-$	0.032	3759.3(5)	$7/2^-$
			3767.2(2)	30(4)	3	$7/2^-$	0.13	3767.2(4)	$7/2^-$

TABLE I. (*Continued.*)

(n,γ)			(d,p)					Adopted	
Level energy (keV)	ΣI_γ (in)[a] per 100n	ΣI_γ (out)[a] per 100n	Level energy[b] (keV)	$\frac{d\sigma}{d\Omega}$ at 20° ($\frac{\mu b}{sr}$)	l	J^π	S_{dp} ($\times$100)	Level energy (keV)	J^π
			3771.3(2)	16(4)	3	$7/2^-$	0.12	3771.3(4)	$7/2^-$
3789.0(2)	0.11(7)	0.10(3)	3788.6(1)	7.3(7)	1	$3/2^-$	0.14	3789.0(2)	$3/2^-$
			3796.1(3)	7.8(21)[h]	1	$1/2^-$	0.17	3796.1(4)	$1/2^-$
3806.8(1)	1.77(11)	1.74(9)	3806.4(1)	91(2)	1	$3/2^-$	1.5	3806.8(1)	$3/2^-$
			3818.5(5)	13(2)	(3)	$(5/2^-)$	0.068	3818.5(6)	$(5/2^-)$
3829.0(1)	1.13(4)	1.20(6)	3828.8(1)	87(3)	1	$3/2^-$	1.2	3829.0(1)	$3/2^-$
			3835.8(2)	30(2)	3	$5/2^-$	0.21	3835.8(3)	$5/2^-$
3843.6(1)	1.13(4)	0.93(4)	3843.1(1)	60(2)	1	$3/2^-$	0.95	3843.6(1)	$3/2^-$
			3850.3(2)	21(2)	3	$7/2^-$	0.091	3850.3(4)	$7/2^-$
3861.0(1)	1.85(4)	1.62(7)	3860.2(1)	113(4)	1	$1/2^-$	3.4	3861.0(1)	$1/2^-$
			3867.7(1)	67(3)	3	$7/2^-$	0.27	3167.7(3)	$7/2^-$
			3876.7(2)	9.2(16)	3	$5/2^-$	0.081	3876.7(4)	$5/2^-$
			3884.3(2)	12(2)	2(3)	$5/2^+(7/2^-)$	0.11	3884.3(4)	$5/2^+(7/2^-)$
			3892.2(1)	26(2)	3	$5/2^-$	0.16	3892.1(3)	$5/2^-$
3906.8(2)	0.35(3)	0.22(4)	3906.2(1)	19(4)	1	$1/2^-$	0.68	3906.8(2)	$1/2^-$
			3910.4(3)	9.8(48)	1	$3/2^-$	0.17	3910.4(4)	$3/2^-$
			3919.8(3)	6.2(16)	5	$9/2^-$	0.21	3919.8(4)	$9/2^-$
			3923.9(1)	26(2)	5	$9/2^-$	0.89	3923.9(3)	$9/2^-$
			3937.2(1)	18(2)	5	$9/2^-$	0.67	3937.2(3)	$9/2^-$
			3945.3(2)	10(1)	1	$1/2^-$	0.34	3945.3(4)	$1/2^-$
3951.0(2)	0.48(19)	0.28(2)	3951.4(1)	26(2)	1	$3/2^-$	0.45	3951.0(2)	$3/2^-$
			3958.6(1)	97(3)	3	$7/2^-$	0.41	3958.6(4)	$7/2^-$
			3964.9(5)	2.4(12)[i]	(3)	$(7/2^-)$	0.041	3964.9(6)	$(7/2^-)$
			3979.5(2)	9.1(14)	3	$7/2^-$	0.041	3979.5(4)	$7/2^-$
			3988.2(1)	6.3(15)	5	$9/2^-$	0.20	3988.2(3)	$9/2^-$
			4002.6(1)	19(2)	(1)	$(3/2^-)$	0.23	4002.6(3)	$(3/2^-)$
4009.1(1)	8.9(1)	8.6(1)	4008.8(1)	357(15)	1	$1/2^-$	11	4009.1(1)	$1/2^-$
			4012.4(1)	28(15)	1	$1/2^-$	1.7	4012.4(3)	$1/2^-$
4023.0(1)	8.7(1)	8.8(1)	4022.7(1)	380(25)	1	$1/2^-$	12	4023.0(1)	$1/2^-$
4026.9(2)	0.24(16)	0.12(3)	4026.5(1)	142(25)	1	$1/2^-$	4.5	4026.9(2)	$1/2^-$
			4038.9(2)	15(3)	3	$5/2^-$	0.090	4038.9(4)	$5/2^-$
4049.6(2)	0.68(2)	0.74(7)	4049.2(1)	75(3)	1	$3/2^-$	1.1	4049.6(2)	$3/2^-$
			4055.0(1)	105(3)	5	$9/2^-$	3.8	4055.0(3)	$9/2^-$
4064.9(2)	0.12(6)	0.11(3)						4064.9(2)	$1/2^-$,$3/2^-$
			4065.4(1)	26(4)	4	$9/2^+$	0.14	4065.4(3)	$9/2^+$
4069.4(1)	0.69(2)	0.40(3)	4069.3(1)	40(4)	1	$3/2^-$	0.52	4069.4(1)	$3/2^-$
			4077.5(3)	80(21)	3	$7/2^-$	0.032	4077.5(4)	$7/2^-$
			4083.9(1)	18(2)	1	$1/2^-$	0.39	4083.9(3)	$1/2^-$
4091.8(1)	0.90(2)	0.81(7)	4091.5(1)	53(2)	1	$3/2^-$	0.85	4091.8(1)	$3/2^-$
			4098.1(2)	12(2)	3	$7/2^-$	0.042	4098.1(4)	$7/2^-$
			4113.8(1)	33(4)	3	$5/2^-$	0.23	4113.8(4)	$5/2^-$
			4118.9(1)	38(4)	5	$9/2^-$	1.2	4118.9(3)	$9/2^-$
			4125.6(2)	34(3)	3	$7/2^-$	0.12	4125.6(4)	$7/2^-$
4130.6(2)	0.43(9)	0.31(5)						4130.6(2)	$3/2^-$
			4131.3(1)	62(3)	(4)	$(9/2^+)$	0.26	4131.3(3)	$(9/2^+)$
			4145.2(3)	13(8)[g]	(3)	$(5/2^-)$	0.27	4145.2(4)	$(5/2^-)$
			4146.9(1)	84(3)	3	$5/2^-$	0.49	4146.9(3)	$5/2^-$
4150.3(2)	0.27(3)	0.45(6)						4150.3(2)	$1/2^-$,$3/2^-$
4154.6(2)	0.21(11)	0.19(4)						4154.6(2)	$1/2^-$,$3/2^-$
			4154.8(1)	41(2)	4	$9/2^+$	0.18	4154.8(3)	$9/2^+$
4163.5(1)	1.55(5)	1.30(5)	4163.5(1)	95(3)	1	$3/2^-$	1.7	4163.5(1)	$3/2^-$
			4173.4(3)	9.0(16)	(1)	$(1/2^-)$	0.39	4173.4(5)	$(1/2^-)$
			4181.8(2)	13(2)	3	$7/2^-$	0.056	4181.8(4)	$7/2^-$
4190.7(1)	1.3(10)	1.07(9)						4190.7(1)	$3/2^-$
			4192.4(1)	441(6)	3	$5/2^-$	2.6	4192.4(3)	$5/2^-$

TABLE I. (*Continued.*)

(n,γ)			(d,p)					Adopted	
Level energy (keV)	ΣI_γ (in)[a] per 100n	ΣI_γ (out)[a] per 100n	Level energy[b] (keV)	$\frac{d\sigma}{d\Omega}$ at 20° ($\frac{\mu b}{sr}$)	l	J^π	S_{dp} ($\times$100)	Level energy (keV)	J^π
4195.4(2)	0.31(2)	0.29(3)						4195.4(2)	$1/2^-$,$3/2^-$
			4196.2(3)	32(7)[e f g h i j]	(3)	$(7/2^-)$	0.047	4196.2(4)	$(7/2^-)$
4209.7(2)	0.15(2)	0.07(1)						4209.7(2)	$1/2^-$,$3/2^-$
			4210.1(1)	41(3)	5	$9/2^-$	1.1	4210.1(3)	$9/2^-$
			4222.4(1)	17(2)	5	$9/2^-$	0.55	4222.4(3)	$9/2^-$
			4231.7(2)	11(2)	5	$9/2^-$	0.37	4231.7(4)	$9/2^-$
			4240.6(1)	73(3)	3	$5/2^-$	0.42	4240.6(3)	$5/2^-$
			4247.2(1)	85(6)	3	$5/2^-$	0.51	4247.2(3)	$5/2^-$
			4250.1(3)	26(8)	(5)	$(9/2^-)$	0.85	4250.1(4)	$(9/2^-)$
			4258.8(1)	163(4)	3	$5/2^-$	1.0	4258.8(3)	$5/2^-$
4269.8(2)	0.40(17)	0.18(2)	4269.7(1)	27(3)	1	$3/2^-$	0.57	4269.8(2)	$3/2^-$
4278.0(2)	0.21(2)	0.09(1)	4277.9(2)	9.3(11)[e]	1	$1/2^-$	0.43	4278.0(2)	$1/2^-$
4285.8(2)	0.89(15)	0.91(4)	4286.1(1)	53(2)	1	$3/2^-$	1.0	4285.8(2)	$3/2^-$
			4299.4(1)	20(1)	3	$7/2^-$	0.11	4299.4(3)	$7/2^-$
			4309.6(3)	28(5)	(3)	$(7/2^-)$	0.11	4309.6(4)	$(7/2^-)$
4311.8(2)?	0.04(2)	0.04(1)						4311.8(2)?	$1/2^-$,$3/2^-$
4313.3(2)	0.37(2)	0.39(6)	4313.4(1)	52(6)	1	$3/2^-$	0.91	4313.3(2)	$3/2^-$
4322.4(2)	0.35(2)	0.30(6)	4322.9(1)	29(1)	1	$3/2^-$	0.47	4322.4(2)	$3/2^-$
			4338.6(2)	13(2)	3	$7/2^-$	0.054	4338.6(4)	$7/2^-$
			4343.3(1)	19(3)	3	$5/2^-$	0.11	4343.3(3)	$5/2^-$
4357.0(2)	0.26(13)	0.14(5)	4357.5(1)	7.4(10)[e]	1,3	$1/2^-$,$5/2^-$	0.34	4357.0(2)	$(1/2^-)$
			4367.5(1)	20(2)	3	$5/2^-$	0.14	4367.5(3)	$5/2^-$
			4374.4(1)	15(3)	(3)	$7/2^-$	0.062	4374.4(3)	$7/2^-$
4383.8(2)	0.34(2)	0.19(3)	4384.1(1)	15(2)	1	$1/2^-$	0.55	4383.8(2)	$1/2^-$
			4389.5(1)	27(2)	3	$5/2^-$	0.14	4389.5(3)	$5/2^-$
			4398.1(4)	3.3(8)	(5)	$(9/2^-)$	0.12	4398.1(5)	$(9/2^-)$
4410.0(2)	0.10(5)	0.16(2)	4410.9(1)	30(2)[e]	1	[c]	0.31	4410.0(2)	$3/2^-$
4412.4(2)	0.33(16)	0.20(5)	4410.9(1)		1	[c]	0.64	4412.4(2)	$1/2^-$
			4418.0(1)	28(2)[e]	5	$9/2^-$	1.2	4418.0(3)	$9/2^-$
4423.0(2)	0.15(5)	0.19(4)	4423.1(1)	27(2)[e]	1	$(3/2^-)$	0.59	4423.0(2)	$3/2^-$
4432.5(2)	0.46(7)	0.13(3)	4432.3(1)	24(2)[e]	1	$3/2^-$	0.47	4432.5(2)	$3/2^-$
			4438.1(1)	26(2)[e]	3	$5/2^-$	0.35	4438.1(3)	$5/2^-$
4446.5(2)	0.17(3)	0.22(7)	4445.9(2)	19(8)[e]	1	$3/2^-$	0.28	4446.5(2)	$3/2^-$
4451.2(2)	0.16(2)	0.06(1)	4450.2(2)	11(3)[e]	1	$1/2^-$	0.43	4451.2(2)	$1/2^-$
			4457.8(3)	5.0(11)[e]	1	$3/2^-$	0.13	4457.8(4)	$3/2^-$
			4466.4(5)	6.0(20)[e]	(1)	$(3/2^-)$	0.18	4466.4(6)	$(3/2^-)$
4469.3(2)	0.51(15)	0.62(10)	4470.9(1)	44(3)	1	$3/2^-$	0.90	4469.3(2)	$3/2^-$
			4485.2(1)	34(4)	3	$7/2^-$	0.15	4485.2(3)	$7/2^-$
			4492.2(4)	12(5)	(3)	$(7/2^-)$	0.073	4492.2(5)	$(7/2^-)$
4496.9(1)	0.69(15)	0.77(6)	4497.5(1)	85(7)	1	$3/2^-$	1.6	4496.9(1)	$3/2^-$
			4504.6(1)	17(3)	3	$7/2^-$	0.081	4504.6(3)	$7/2^-$
			4513.9(4)	6.2(37)	1	$1/2^-$	0.29	4513.9(5)	$1/2^-$
			4519.7(2)	28(4)	3	$5/2^-$	0.19	4519.7(4)	$5/2^-$
4523.4(3)	0.09(6)	0.08(2)						4523.4(3)	$1/2^-$,$3/2^-$
			4525.7(2)	31(4)	3	$7/2^-$	0.12	4525.7(4)	$7/2^-$
4536.6(2)	0.96(2)	1.0(2)	4537.1(1)	69(6)	1	$1/2^-$	2.7	4536.6(2)	$1/2^-$
4540.6(2)	0.12(2)	0.14(3)						4540.6(2)	$1/2^-$,$3/2^-$
			4544.6(1)	78(6)	3	$5/2^-$	0.49	4544.6(4)	$5/2^-$
			4553.6(2)	28(3)	2	$5/2^+$	0.13	4553.6(4)	$5/2^+$
4559.5(2)	0.36(7)	0.23(5)	4560.6(2)	16(3)[h]	1	$1/2^-$	0.63	4559.5(2)	$1/2^-$
			4563.8(4)?					4563.8(5)?	
4565.0(3)?	0.17(4)	0.05(2)						4565.0(3)?	$1/2^-$,$3/2^-$
			4572.3(1)	120(14)	3	$5/2^-$	0.90	4572.3(4)	$5/2^-$
			4575.9(4)	39(14)	(3)	$(5/2^-)$	0.23	4575.9(5)	$(5/2^-)$
4594.4(3)	0.14(8)	0.04(1)						4594.4(3)	$1/2^-$,$3/2^-$

TABLE I. (*Continued.*)

(n,γ)			(d,p)					Adopted	
Level energy (keV)	ΣI_γ (in)[a] per 100n	ΣI_γ (out)[a] per 100n	Level energy[b] (keV)	$\frac{d\sigma}{d\Omega}$ at 20° ($\frac{\mu b}{sr}$)	l	J^π	S_{dp} ($\times$100)	Level energy (keV)	J^π
			4596.2(1)	44(4)	5	$9/2^-$	1.3	4596.2(4)	$9/2^-$
			4601.2(1)	55(4)	5	$9/2^-$	1.7	4601.2(4)	$9/2^-$
4602.5(3)	0.10(6)	0.03(1)						4602.5(3)	$1/2^-$,$3/2^-$
4606.1(2)	0.14(2)	0.18(4)						4606.1(2)	$1/2^-$,$3/2^-$
			4607.9(2)	16(2)	5	$9/2^-$	0.58	4607.9(4)	$9/2^-$
			4615.9(1)	20(2)	3	$5/2^-$	0.12	4615.9(4)	$5/2^-$
			4624.8(1)	121(3)	3	$5/2^-$	0.61	4624.8(4)	$5/2^-$
4634.2(2)	0.31(12)	0.13(3)	4633.6(6)	6.0(21)[j]	(1)			4634.2(2)	$1/2^-$,$3/2^-$
			4639.0(1)	189(6)	3	$5/2^-$	1.1	4639.0(4)	$5/2^-$
4644.3(2)	0.11(3)	0.08(3)						4644.3(2)	$1/2^-$,$3/2^-$
			4644.6(1)	59(5)	5	$9/2^-$	1.9	4644.6(4)	$9/2^-$
4646.8(2)	0.18(2)	0.19(2)						4646.8(2)	$1/2^-$,$3/2^-$
			4651.0(1)	178(4)	3	$5/2^-$	1.0	4651.0(4)	$5/2^-$
4658.7(3)?	0.09(3)	0.01(1)						4658.7(3)?	$1/2^-$,$3/2^-$
			4664.9(1)	47(2)	3	$(7/2^-)$	0.18	4664.9(5)	$(7/2^-)$
			4675.8(1)	27(3)	3	$7/2^-$	0.14	4675.8(5)	$7/2^-$
			4689.1(1)	72(6)	3	$7/2^-$	0.28	4689.1(5)	$7/2^-$
4691.3(2)	0.32(3)	0.12(3)						4691.3(2)	$1/2^-$,$3/2^-$
			4693.7(1)	91(6)	3	$5/2^-$	0.57	4693.7(5)	$5/2^-$
4695.3(2)	0.20(3)	0.10(2)						4695.3(2)	$1/2^-$,$3/2^-$
			4699.0(1)	34(4)	3	$5/2^-$	0.24	4699.0(5)	$5/2^-$
			4710.6(1)	259(6)	3	$5/2^-$	1.5	4710.6(5)	$5/2^-$
4711.1(2)	0.06(3)	0.07(2)						4711.1(2)	$1/2^-$,$3/2^-$
4712.8(2)	0.13(6)	0.14(1)						4712.8(2)	$1/2^-$,$3/2^-$
			4718.3(1)	315(6)	3	$5/2^-$	1.9	4718.3(5)	$5/2^-$
4725.1(2)	0.70(13)	1.02(4)	4725.0(1)	109(4)	1	$1/2^-$	3.9	4725.1(2)	$1/2^-$
4734.6(2)	0.17(3)	0.18(4)	4734.1(1)	35(3)	1	$3/2^-$	0.66	4734.6(2)	$3/2^-$
			4743.9(1)	128(4)	3	$5/2^-$	0.74	4743.9(5)	$5/2^-$
4749.7(3)?	0.09(4)	0.01(1)						4749.7(3)?	$1/2^-$,$3/2^-$
			4756.3(2)	19(12)	5	$9/2^-$	0.76	4756.3(6)	$9/2^-$
			4760.3(1)	157(10)	3	$5/2^-$	1.0	4760.3(5)	$5/2^-$
4762.8(2)	0.12(6)	0.11(3)						4762.8(2)	$3/2^-$
			4763.9(4)	26(8)	(5)	$(9/2^-)$	0.98	4763.9(7)	$(9/2^-)$
			4771.1(2)	33(3)	5	$9/2^-$	0.89	4771.1(6)	$9/2^-$
4775.7(3)	0.13(6)	0.03(1)						4775.7(3)	$1/2^-$,$3/2^-$
4777.0(3)	0.04(2)	0.04(1)						4777.0(3)	$1/2^-$,$3/2^-$
			4778.3(1)	120(14)	3	$5/2^-$	0.75	4778.3(5)	$5/2^-$
			4799.6(1)	51(45)	3	$5/2^-$	0.74	4799.6(6)	$5/2^-$
			4801.8(1)	156(44)	(5)	$(9/2^-)$	3.0	4801.8(6)	$(9/2^-)$
4805.3(2)	0.20(2)	0.04(1)						4805.3(2)	$1/2^-$,$3/2^-$
			4808.2(1)	119(4)	3	$5/2^-$	0.61	4808.2(6)	$5/2^-$
			4814.4(1)	69(3)	5	$9/2^-$	1.9	4814.4(6)	$9/2^-$
4814.5(2)	0.20(2)	0.13(3)						4814.5(2)	$3/2^-$
4824.7(2)	0.22(5)	0.13(2)						4824.7(2)	$3/2^-$
			4825.0(1)	87(3)	3	$5/2^-$	0.52	4825.0(6)	$5/2^-$
			4832.1(1)	150(3)	3	$5/2^-$	0.83	4832.1(6)	$5/2^-$
			4847.0(1)	93(3)	3	$5/2^-$	0.51	4847.0(6)	$5/2^-$
4849.3(3)	0.04(4)	0.04(1)						4849.3(3)	$1/2^-$,$3/2^-$
			4854.1(1)	24(2)	3	$5/2^-$	0.16	4854.1(6)	$5/2^-$
4855.9(3)	0.07(4)	0.04(1)						4855.9(3)	$1/2^-$,$3/2^-$
			4865.5(1)	51(3)	3	$5/2^-$	0.27	4865.5(6)	$5/2^-$
4871.5(3)	0.11(4)	0.04(1)						4871.5(3)	$1/2^-$,$3/2^-$
			4872.5(1)	113(3)	3	$5/2^-$	0.61	4872.5(6)	$5/2^-$
			4875.7(4)	20(7)[e]				4875.7(7)	
			4880.9(2)	32(2)	3	$5/2^-$	0.17	4880.9(6)	$5/2^-$

TABLE I. (*Continued.*)

(n,γ)			(d,p)					Adopted	
Level energy (keV)	ΣI_γ (in)[a] per 100n	ΣI_γ (out)[a] per 100n	Level energy[b] (keV)	$\frac{d\sigma}{d\Omega}$ at 20° ($\frac{\mu b}{sr}$)	l	J^π	S_{dp} ($\times$100)	Level energy (keV)	J^π
			4892.4(1)	47(2)	3	$5/2^-$	0.24	4892.4(6)	$5/2^-$
4892.8(4)?		0.04(1)						4892.8(4)?	$1/2^-$,$3/2^-$
4898.0(2)	0.17(4)	0.11(2)						4898.0(2)	$3/2^-$
			4900.0(1)	75(4)	3	$5/2^-$	0.39	4900.0(7)	$5/2^-$
			4905.7(1)	55(4)	3	$5/2^-$	0.29	4905.7(7)	$5/2^-$
4906.4(2)	0.20(6)	0.20(5)						4906.0(2)	$1/2^-$,$3/2^-$
			4915.2(2)	46(4)	3	$5/2^-$	0.23	4915.2(7)	$5/2^-$
			4919.7(3)	30(4)	3	$5/2^-$	0.16	4919.7(7)	$5/2^-$
			4925.3(3)	27(3)	4	$9/2^+$	0.090	4925.3(7)	$9/2^+$
			4930.2(5)	6.7(34)[e]	4	$9/2^+$	0.047	4930.2(8)	$9/2^+$
			4941.4(1)	24(3)[e]	3	$5/2^-$	0.23	4941.4(7)	$5/2^-$
			4946.3(2)	20(3)[e]	3	$5/2^-$	0.16	4946.3(7)	$5/2^-$
4952.0(2)	0.12(3)	0.06(1)						4952.0(2)	$1/2^-$,$3/2^-$
			4952.8(1)	33(4)[e]	4	$9/2^+$	0.17	4952.8(3)	$9/2^+$
			4955.9(3)	31(6)	(4)	$(9/2^+)$	0.10	4955.9(4)	$(9/2^+)$
4959.3(6)?	0.08(3)	0.01(1)						4959.3(6)?	$1/2^-$,$3/2^-$
			4962.6(1)	34(3)[e]	4	$9/2^+$	0.16	4962.6(7)	$9/2^+$
4963.7(2)	0.16(3)	0.06(1)						4963.7(2)	$1/2^-$,$3/2^-$
			4968.5(1)	38(11)[e]	3	$5/2^-$	0.32	4968.5(7)	$5/2^-$
4972.6(2)	0.06(5)	0.13(3)						4972.6(2)	$1/2^-$,$3/2^-$
			4972.7(1)	66(13)[e]	3	$5/2^-$	0.62	4972.7(7)	$5/2^-$
			4978.1(6)?	21(17)				4978.1(9)?	
4979.5(3)	0.09(6)	0.01(1)	4980.6(2)	21(3)[e]	1	$3/2^-$	0.80	4979.5(3)	$3/2^-$
			4990.6(1)	29(2)[e]	5	$9/2^-$	0.89	4990.6(7)	$9/2^-$
			4998.0(1)	34(3)[e]	5	$(9/2^-)$	0.78	4998.0(7)	$(9/2^-)$
5002.5(5)	0.05(2)	0.01(1)						5002.5(5)	$1/2^-$,$3/2^-$
			5011.5(1)	85(7)	3	$5/2^-$	0.59	5011.5(7)	$5/2^-$
			5016.4(2)	54(6)	3	$5/2^-$	0.23	5016.4(8)	$5/2^-$
			5028.2(5)	11(2)[e]	5	$9/2^-$	0.33	5028.2(9)	$9/2^-$
5033.2(3)	0.30(11)	0.04(1)	5034.8(1)	66(6)	1	[d]	2.0	5033.2(3)	$1/2^-$
5037.1(3)	0.14(6)	0.02(1)	5034.8(1)		1	[d]	0.66	5037.1(3)	$(3/2^-)$
			5039.7(2)	43(5)	5	$9/2^-$	1.2	5039.7(8)	$9/2^-$
			5046.9(1)	41(5)	5	$9/2^-$	1.3	5046.9(8)	$9/2^-$
5047.8(3)?	0.13(4)	0.02(1)						5047.8(3)?	$1/2^-$,$3/2^-$
			5053.7(3)	32(4)[e]	4	$9/2^+$	0.20	5053.7(8)	$9/2^+$
5054.9(3)?	0.10(4)	0.01(1)						5054.9(3)?	$1/2^-$,$3/2^-$
			5058.1(1)	65(7)	1	$1/2^-$	3.9	5058.1(8)	$1/2^-$
5064.3(3)?	0.07(1)	0.02(1)						5064.3(3)?	$1/2^-$,$3/2^-$
			5065.3(1)	49(36)[e]	3	$5/2^-$	0.47	5065.3(8)	$5/2^-$
5069.5(3)	0.13(4)	0.05(1)						5069.5(3)	$1/2^-$,$3/2^-$
			5073.3(2)	22(3)[e]	3	$5/2^-$	0.16	5073.3(8)	$5/2^-$
			5082.2(2)	30(4)[e]	5	$9/2^-$	0.89	5082.2(8)	$9/2^-$
5083.1(2)	0.31(13)	0.08(2)						5083.1(2)	$1/2^-$,$3/2^-$
			5098.5(1)	18(3)	5	$9/2^-$	0.69	5098.5(8)	$9/2^-$
5100.3(2)	0.07(5)	0.05(1)						5100.3(2)	$1/2^-$,$3/2^-$
			5112.7(1)	53(4)	3	$5/2^-$	0.34	5112.7(8)	$5/2^-$
			5119.9(1)	94(5)	3	$5/2^-$	0.56	5119.9(8)	$5/2^-$
			5125.6(1)	63(4)	4(5)	$9/2^+(9/2^-)$	0.22	5125.6(8)	$9/2^+(9/2^-)$
			5139.9(2)	15(4)	(1)	$(1/2^-)$	0.87	5139.9(9)	$(1/2^-)$
			5144.5(8)	5.6(21)[g]				5144.5(12)	
5153.4(2)	0.06(2)	0.04(1)	5151.1(1)	60(7)	(1)	$(1/2^-)$	2.9	5153.4(2)	$(1/2^-)$
			5157.6(4)	13(2)[e]				5157.6(4)	
5159.6(5)?		0.02(1)						5159.6(5)?	$1/2^-$,$3/2^-$
			5162.1(2)	33(2)[e]	3	$5/2^-$	0.49	5162.1(9)	$5/2^-$
5168.2(4)?	0.05(2)	0.01(1)						5168.2(4)?	$1/2^-$,$3/2^-$

TABLE I. (*Continued.*)

(n,γ)			(d,p)					Adopted	
Level energy (keV)	ΣI_γ (in)[a] per 100n	ΣI_γ (out)[a] per 100n	Level energy[b] (keV)	$\frac{d\sigma}{d\Omega}$ at 20° ($\frac{\mu b}{sr}$)	l	J^π	S_{dp} ($\times$100)	Level energy (keV)	J^π
			5169.6(2)	22(1)[e]	3	$5/2^-$	0.30	5169.6(9)	$5/2^-$
			5176.8(1)	22(1)[e]	1	$1/2^-$	1.4	5176.8(9)	$1/2^-$
			5185.1(2)	37(2)[e]	3	$5/2^-$	0.54	5185.1(9)	$5/2^-$
			5192.0(2)	23(2)[e]	3	$5/2^-$	0.33	5192.0(9)	$5/2^-$
			5196.8(4)	16(2)[e]	(3)	$(5/2^-)$	0.18	5196.8(10)	$(5/2^-)$
5204.6(2)	0.03(2)	0.09(2)	5202.8(2)	14(1)[e]	1	$1/2^-$	1.1	5204.6(2)	$(1/2^-)$
			5213.5(2)	7.3(13)[e]				5213.5(9)	
			5219.5(2)	6.7(13)[e]	(3)	$(5/2^-)$	0.11	5219.5(10)	$(5/2^-)$
			5228.1(1)	28(2)[e]	3	$5/2^-$	0.36	5228.1(9)	$5/2^-$
			5232.9(1)	42(2)[e]	3	$5/2^-$	0.54	5232.9(9)	$5/2^-$
			5245.9(4)	5.4(26)[e]	1	$3/2^-$	0.24	5245.9(10)	$3/2^-$
			5254.1(2)	8.4(46)[e]	(3)	$(5/2^-)$	0.15	5254.1(10)	$(5/2^-)$
5269.5(2)	0.05(2)	0.04(1)						5269.5(2)	$1/2^-$,$3/2^-$
			5269.6(1)	67(11)	3	$5/2^-$	0.32	5269.6(10)	$5/2^-$
			5275.6(5)	7.9(33)[g]	(3)	$(5/2^-)$	0.16	5275.6(11)	$(5/2^-)$
			5280.1(1)	27(8)	3	$5/2^-$	0.16	5280.1(10)	$5/2^-$
			5285.7(2)	13(9)	(6)	$(13/2^+)$	0.49	5285.7(10)	$(13/2^+)$
5286.3(2)	0.20(5)	0.02(1)						5286.3(2)	$1/2^-$,$3/2^-$
5299.1(5)?	0.02(2)	0.02(1)						5299.1(5)?	$1/2^-$,$3/2^-$
5306.4(4)	0.08(3)	0.02(1)						5306.4(4)	$1/2^-$,$3/2^-$
5316.8(3)	0.04(3)	0.02(1)						5316.8(3)	$1/2^-$,$3/2^-$
5322.7(4)	0.04(2)	0.03(1)						5322.7(4)	$1/2^-$,$3/2^-$
5336.9(2)	0.04(2)	0.04(1)						5336.9(2)	$1/2^-$,$3/2^-$

[a]Internal conversion is included.
[b]Only statistical error is given. For total uncertainties the systematic error of 0.3 keV should be added in quadrature. Above 4.5 MeV this systematic error linearly increases up to 1.0 keV at 5.3 MeV.
[c]Unresolved doublet of 4410.0 keV $3/2^-$ and 4412.4 keV $1/2^-$ states. Spectroscopic factors were divided into two components by fitting the asymmetry.
[d]Unresolved doublet of 5033.2 keV $1/2^-$ and 5037.1 keV $(3/2^-)$ states. Spectroscopic factors were divided into two components by fitting the asymmetry.
[e f g h i j]Partial cross section at scattering angle 30°, 25°, 35°, 15°, 40°, and 45°, respectively.
[k]From coupled-channel Born approximation (CCBA) analysis.

3. *Discussion of uncertainties of extracted spectroscopic factors*

Uncertainties of the extracted spectroscopic factors can stem from experimental errors of differential cross sections and from model dependency of these spectroscopic factors. In this subsection we summarize and discuss these uncertainties.

As can be seen from the fifth column of Table I and Figs. 3–7, statistical errors of differential cross sections of most of the levels are low. Mainly due to uncertainty of the target thickness a possible systematic error of about 15% should be added to these statistical errors.

Another source of uncertainty of a spectroscopic factor could be the coupled-channel effect. This effect was briefly discussed in the previous subsection. It was shown that this effect is negligible for the spherical nucleus ^{125}Sn.

Since $\sigma_{lj}^{\mathrm{CHUCK3}}$ in Eq. (2) depend on the optical-model parameters and the geometric parameters of the Woods-Saxon potentials of the bound states, the spectroscopic factors calculated from Eq. (2) are model dependent. For peripheral reactions these uncertainties can be strongly reduced using the asymptotic normalization coefficient (ANC) of the overlap function of the bound-state wave functions of the initial and final particles. The extraction of the spectroscopic factors using ANC's was described in works [33,34].

While the absolute values of the DWBA calculated partial cross section depend relatively weakly on the optical-model parameters for deuteron and proton the geometric parameters of the Woods-Saxon potentials of the bound states can lead to the large uncertainties of the calculated partial cross section. These geometric parameters are not well determined from experimental data. As can be seen from Table III this ambiguity can result in uncertainties of the partial cross sections in order of several tens of percent.

Some uncertainties can follow also from not well established corrections for the zero-range interaction and local potentials. But these corrections should not exceed 10%

[35,36]. In the present work the recommended finite range correction 0.621 and nonlocality parameter *nlc* listed in Table II were used.

Considering these uncertainties we compare the extracted spectroscopic factors from the present work with those from the previous works on this isotope [9,15,31,37,38]. In Table IV the four representative spectroscopic factors from our work are compared with the results from the previous works. Our extracted spectroscopic factors are systematically smaller than those reported in the earlier (d,p) [9,31] works as well as in the experiment in reverse kinematics performed recently in Oak Ridge [38]. Nevertheless, taking into account the uncertainties mentioned above, our spectroscopic factors for the ground state and the first $1/2^+$ state are not in contradiction with the previous results. The larger differences between our and previous results for the 2.755-keV state can be, at least partly, explained by worse energy resolutions in previous works. Subtracting the contribution of $7/2^-$ states at 2.797 and 2.893 keV in the Oak Ridge measurement [38] one arrives at a similar ratio between our and Oak Ridge spectroscopic factors as for the ground state and the first $1/2^+$ state. The parameters of the optical model cannot elucidate this systematic lowering of our spectroscopic factors with respect to previous work [9,31,38]. These parameters were the same or very similar in all these works. Thus the only possible explanation of this systematic discrepancy might be our target thickness uncertainty, which was mentioned above. However, the relative good agreement with values in works by Schneid *et al.* [37] and Massolo *et al.* [15] prevents us from making such definite conclusion.

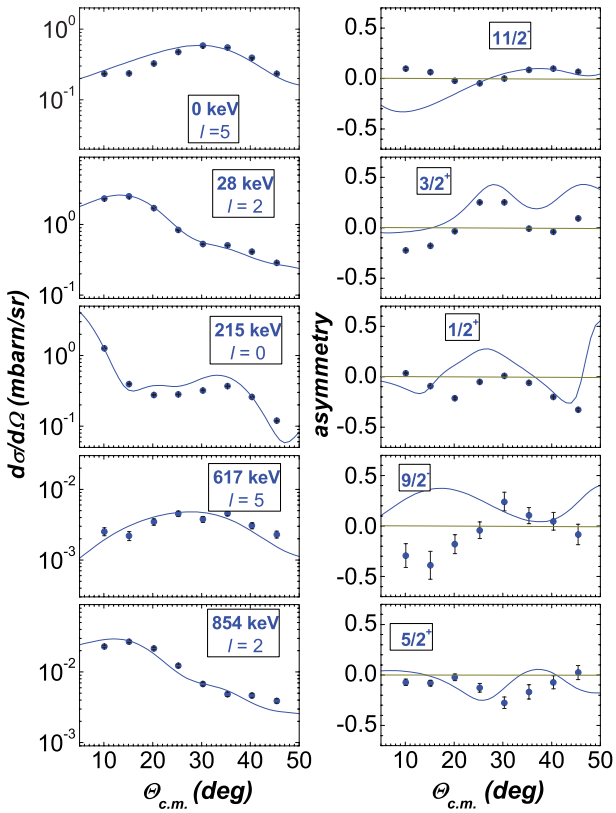

FIG. 3. (Color online) Angular distributions obtained in the ^{124}Sn$(\vec{d},p)^{125}$Sn measurement at $E_d = 22$ MeV. Circles and squares represent experimental data. Lines follow from DWBA calculation.

III. LEVEL AND DECAY SCHEME

A. Construction of level and decay scheme

The level and decay scheme from Ref. [13] was used as the starting point for the construction of the new extended level and decay scheme. For the introduction of a new level, for the placement of a new transition, and for a spin-parity assignment we adopted several rules.

A new level was generally introduced if

(i) we had obtained the evidence for this level in the $(\vec{d},p)$ experiment at least at three angles, or

(ii) at least three independent transitions, which had not been placed yet, had provided evidence in $\gamma-\gamma$ coincidence spectra with an energy precision better than two standard deviations, or

(iii) the weak evidence from one experiment was confirmed by the other.

Questionable levels, which do not fulfill the rules mentioned above or which fulfill them but evidence for them seems to be insufficient, are marked in Table I by a question mark.

The placement of γ transitions was done in several steps. In the first step, we attempted to place the 65 strongest lines. These transitions confirm and extend the level and decay

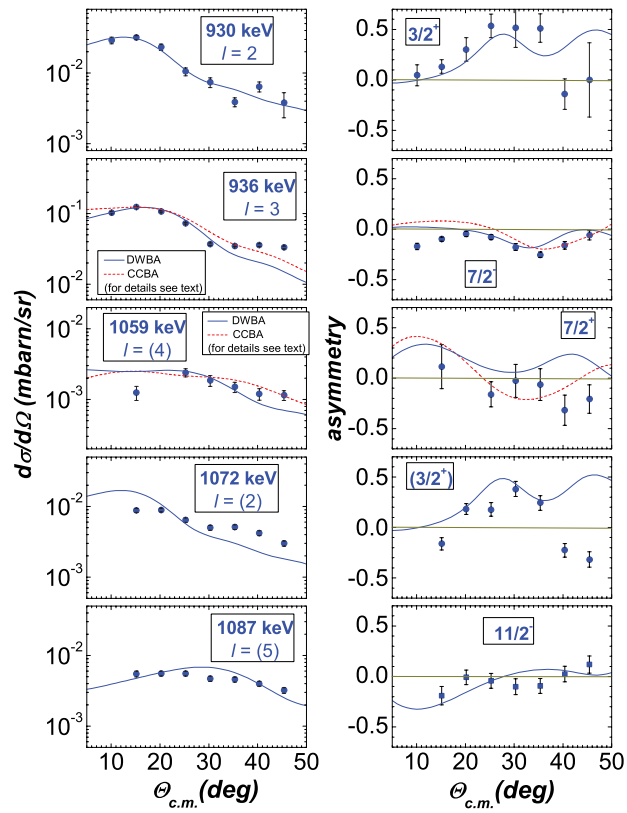

FIG. 4. (Color online) Same caption as for Fig. 3.

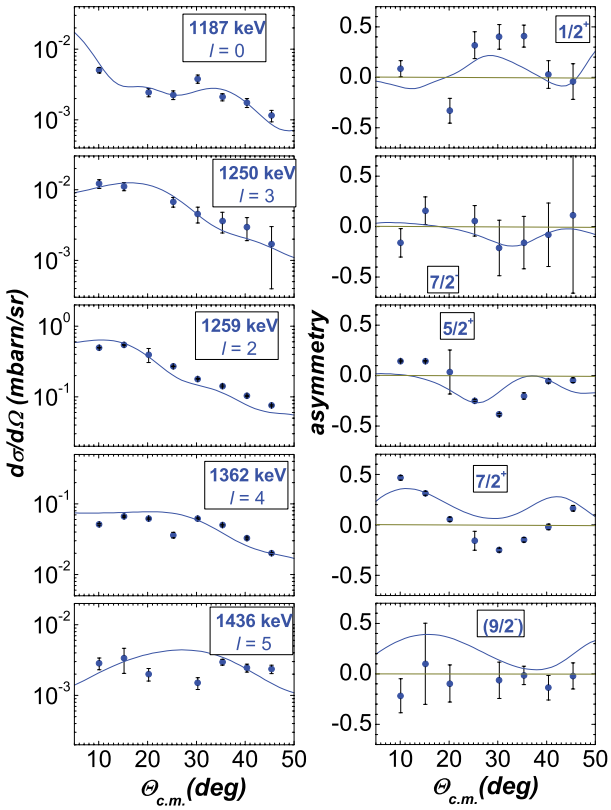

FIG. 5. (Color online) Same caption as for Fig. 3.

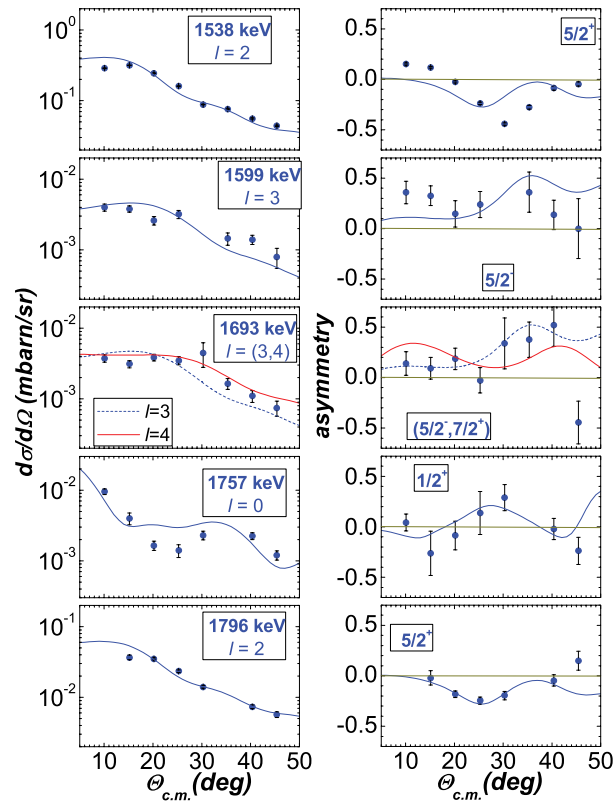

FIG. 6. (Color online) Same caption as for Fig. 3.

scheme from Nuclear Data Sheets [13]. In the next steps we iteratively incorporated γ lines observed in the coincidence spectra. Combining evidences from the large number of the coincidence spectra, 565, we were able to place 747 γ transitions including many close doublets. The set of 166 levels and 747 placed transitions was used as input for the program LEVFIT [39]. This program calculated the final level energies. The γ decay of levels observed in the (n,γ) reaction is presented in Table V and VI.

The spin and parity assignments follow for most of the levels from the DWBA analysis of the (d,p) data. Nevertheless, two criteria for spin and parity restrictions were applied for the (n,γ) data. First, we assumed that levels populated by the primary transitions are $1/2^{\pm}$ or $3/2^{\pm}$. Second, the $E1$, $M1$, or $E2$ multipolarity character is ascribed to the secondary transitions. In most cases, the spin and parity assignment from the (d,p) reaction is not in contradiction with the observation from the (n,γ) reaction. In cases of disagreement, we proposed level doublets.

B. Discussion of the level and decay scheme

The performed experiments yielded about 400 levels in the region up to the neutron binding energy. Most of them are newly observed levels. One of the goals of this work is to construct a complete level and decay scheme in the region of low-lying levels. With the experience of the neighboring Te isotopes we propose the essentially complete level scheme in a spin range up to 7/2 and an excitation energy range up to 1.9 MeV including spin-parity assignment and decay mode. Compared with the latest NDS compilation [13] we established 11 new levels and found new spin-parity assignment for five levels in this region. There is only one questionable level at 1747 keV and one level, 1684 keV, with an ambiguous spin-parity assignment. In the coincidence spectra we observed three γ transitions depopulating the 1747-keV level. All three transitions fit in the decay scheme well. Nevertheless, the lack of any γ transitions populating this level and no evidence in the (d,p) reaction prevent us from establishing this level firmly.

In the low-energy part of the level scheme most of the newly established levels were clearly observed in both experiments. These levels are well proven. The low-energy excited states observed in the (d,p) reaction are shown in Fig. 8. In this proton spectrum the newly established levels are labeled by a bold font. The close doublet around 1795 keV, which is manifested in the proton spectrum as a slightly broader peak, was confirmed by the (n,γ) experiment; see (a), (b), and (d) coincidence spectra in Fig. 9. Similarly, the $7/2^-$ missing member of the family of negative-parity states built upon the $1h_{11/2}$ orbital at 1250 keV were verified by the γ coincidence spectra. The two most important coincidence spectra for adoption of this level are depicted in Fig. 9(e), and 9(f) spectra. Note that these two coincidence spectra, which are gated by the cascade γ transitions 618 and 632 keV, were very effective also for disclosure of members of this $1h_{11/2}$ family of states at higher excitation energies. In proton spectra we do not observe any evidence for the new level at 1684 keV. However, five depopulating and eight populating γ lines following from the coincidence $(n,\gamma\gamma)$ measurements allow us to introduce this

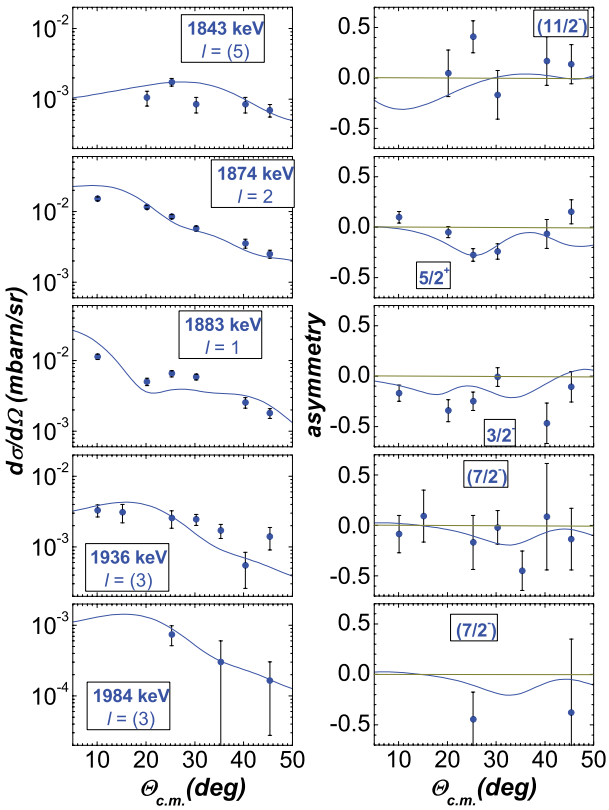

FIG. 7. (Color online) Same caption as for Fig. 3.

level in the level scheme of ^{125}Sn; see, for example, spectra (c) and (d) in Fig. 9.

Another important result of this extensive spectroscopic work is the large number of $7/2^-$, $5/2^-$, $3/2^-$, and $1/2^-$ levels. The sets of these levels gave us the excellent possibility to investigate in detail the distribution of the strength for the $2f_{7/2}$, $2f_{5/2}$, $3p_{3/2}$, and $3p_{1/2}$ subshells. The fragmentation of these strengths will be discussed within the framework of the QPM in the following section.

The very sensitive $(n,\gamma\gamma)$ coincidence experiment produced the very complete decay scheme. Taking into account internal conversion, the sum of the intensities of the observed transitions to the ground state and the isomeric state was (100.7 ± 1.4) γ per 100 neutron captures. Similar completeness was obtained also for the depopulation of the capture state. We were able to see the total capture state depopulation of (96.1 ± 1.3) γ per 100 neutron captures. The completeness of the decay scheme following thermal neutron capture is well documented by the agreement between feeding and outgoing intensity for the well populated levels (see Table I and Figs. 10 and 11). Based on these results one can estimate a rough sensitivity limit for the $(n,\gamma\gamma)$ experiment. We can estimate that all γ transitions with an intensity higher than 0.2γ per 100 neutron captures are disclosed and placed. Exceptions are the transitions from a weakly populated $7/2^+$ state to the 27.5 keV $3/2^+$, for which this threshold is slightly higher.

C. Evaluation of neutron binding energy and isomeric ratio

The level and decay scheme from this work brought two results which deserve special attention. The new and more precise value of the neutron binding energy for ^{125}Sn was evaluated. The fitted value from the program LEVFIT is 5733.47 keV with statistical error 0.12 keV and systematic error 0.10 keV. This value agrees well with the neutron binding energy given in the compilation by Audi *et al.* [40], (5733.1 ± 0.6) keV.

The complete decay scheme enables us to calculate the isomeric ratio between the population of the $11/2^-$ ground state and the isomeric state at 27.5 keV in the $(n_{\rm th},\gamma)$ reaction. Taking into account internal conversion, the ratio was determined to be 0.029 ± 0.006. This ratio can be compared with the ratio of the partial cross sections for the ground and isomeric states. Using the neutron cross sections from the BNL Neutron Cross Section compilation [10] one can obtain the very similar ratio 0.031 ± 0.015. These values are significantly lower than the same ratios for the neighboring odd-A tellurium isotopes [41]. The isomeric ratios between partial cross sections for the $11/2^-$ states and the total cross sections are summarized in Table VII. It should be noted that in this work we report the more precise value of this quantity for ^{131}Te compared to that in Ref. [41]. The explanation for the difference between tellurium isotopes and ^{125}Sn follows from the distribution of $p_{3/2}$ and $p_{1/2}$ strengths. In the case of ^{125}Sn these distributions are situated at higher excitation energies. Therefore the overlap between these distributions and the region with the low-spin member of $h_{11/2}$ family of states is smaller. The smaller admixture of $p_{3/2}$ and $p_{1/2}$ components in the structure of the wave functions of the low-spin member of the $h_{11/2}$ family of states causes the smaller population of the lowest $11/2^-$ state, i.e. the ground state in case of ^{125}Sn.

D. Level density

The nuclear level density is one of the most important statistical properties of a nucleus. Despite many attempts of microscopic calculations of this quantity, the most frequently used formulas are based on simple phenomenological models [42–44], the constant temperature formula (CTF),

$$\rho(E,J) = f(J)\frac{1}{T}e^{(E-E_0)/T}, \qquad (3)$$
$$f(J) = e^{-J^2/2\sigma^2} - e^{-(J+1)^2/2\sigma^2},$$

and the Bethe formula for the back-shifted Fermi gas (BSFG) model,

$$\rho(E,J) = f(J)e^{2\sqrt{a(E-E_1)}}/12\sqrt{2}\sigma a^{1/4}(E-E_1)^{5/4}, \qquad (4)$$

where E is the excitation energy and σ is the spin cutoff parameter. These two formulas use different values of the spin cutoff parameters σ in the spin distribution relation $f(J)$. The constant cutoff parameter $\sigma = 3.97$ for CTF, see [42], and $\sigma^2 = 0.0146A^{5/3}\frac{1+\sqrt{1+4a(E-E_1)}}{2a}$ proposed in Ref. [45] for BSFG were employed. The parameters, T, E_0, a, and E_1 are parameters which are usually fitted to the experimental data.

TABLE II. Optical-model parameters used in DWBA calculations.

V_R (MeV)	r_v (fm)	a_v (fm)	$4W'_D$ (MeV)	r_w (fm)	a_w (fm)	V_{ls} (MeV)	r_{ls} (fm)	a_{ls} (fm)	r_c (fm)	nlc
Deuteron parameters										
114.8	1.16	0.84	44.80	1.35	0.73	7.8	1.16	0.84	1.20	0.54
Proton parameters										
61.6-0.6 E_p	1.245	0.67	52.8	1.245	0.70	8.5	1.245	0.70	1.21	0.85
Bound neutron parameters										
[a]	1.245	0.70				λ =25.0				0.85

[a]Adjusted by the computer program to fit the neutron separation energy.

Following the procedure described in Refs. [42,44], using our level scheme and the average s-wave neutron resonance spacing [44,46] we arrive at the values $T = (0.819 \pm 0.053)$ MeV, $E_0 = (-1.34 \pm 0.35)$ MeV, $a = (11.65 \pm 0.54)$ MeV^{-1}, and $E_1 = (-0.55 \pm 0.24)$ MeV. The fit was performed with 34 levels below 2.2 MeV within the spin range 1/2–7/2. These parameters are in good agreement with the ones in Ref. [44].

The comparison of experimental cumulative numbers of levels with the model predictions of BSFG and CTF is shown in Fig. 12. The experimental data follow the model curves up to 2.7 MeV. Regarding the number of levels within the spin interval 1/2 to 7/2, the level scheme can be considered complete up to this energy. However, many levels above 2.2 MeV are without a unique spin-parity assignment. Therefore the limit of completeness of the level scheme, which is important for testing theoretical models, is considered to be 2.2 MeV.

Besides the phenomenological models CTF and BSFG, we compared the cumulative number of levels with the microscopic prediction of the QPM. This comparison will be discussed in detail below in Sec. IV B.

E. Spin cutoff parameter

The spin cutoff parameter σ determines the spin distribution. It is difficult to obtain this parameter experimentally. The scarce experimental information on this quantity follows from comparison of the total level density at the neutron binding energy with the average spacing of s-wave neutron resonances [47], comparison of a particle angular distribution with statistical model calculation [47–50], and low-lying levels by fitting the spin distribution $f(J)$ in Eq. (3) [42].

This lack of experimental information on the spin cutoff parameters motivated us to extract the spin cutoff parameter from our experimental data. We use two approaches. We made an attempt to extract it from the spin distribution of low-lying levels below the excitation energy of 2.2 MeV and from the distribution of negative parity levels.

TABLE III. Dependence of the DWBA cross sections on the bound-state geometric parameters of Woods-Saxon potentials, r_0 and a_0, for the selected final states. The values of the DWBA cross sections were calculated with the optical-model parameters given in Table II at a scattering angle of 25° except for the $1/2^+$ state at 1757 keV.

r_0 (fm)	a_0 (fm)	0 keV $11/2^-$ (mb/Sr)	28 keV $3/2^+$ (mb/Sr)	1757 keV $1/2^+$[a] (mb/Sr)	2754 keV $7/2^-$ (mb/Sr)	3408 keV $3/2^-$ (mb/Sr)	4026 keV $1/2^-$ (mb/Sr)
1.22	0.67	2.09	2.95	1.63	15.01	4.45	2.43
1.14	0.55	0.91	1.57	1.08	7.77	2.94	1.61
1.14	0.75	1.40	2.43	1.48	12.54	4.23	2.32
1.30	0.55	3.03	3.37	1.69	16.85	4.42	2.42
1.30	0.75	4.18	4.69	2.19	24.47	6.26	3.37

[a]The DWBA cross section at 35°.

TABLE IV. Comparison of four representative spectroscopic factors with results from previous works. In the last two rows the geometric parameters used for the bound states are given.

E_x	nlj	Ref. [37]	Ref. [9]	Ref. [31]	Ref. [15]	Ref. [38]	This work
0.0	$1h_{11/2}$		0.42	0.34	0.30		0.27
0.028	$2d_{3/2}$	0.34	0.44	0.53		0.44	0.30
0.215	$3s_{1/2}$	0.25	0.33	0.32		0.33	0.27
2.755	$2f_{7/2}$		0.54	0.52		0.46	0.30
r_0			1.24	1.245	1.25	1.245	1.245
a_0			0.65	0.70	0.65	0.70	0.70

TABLE V. The γ decay of the levels in ^{125}Sn from the (n,γ) reaction.

E_i(keV)	Spin	E_γ(keV)	I_γ(%)	E_f(keV)	Spin
0.00(0)	11/2−				
27.66(12)	3/2+				
215.22(12)	1/2+				
		187.6	46.37	27.7	3/2+
617.87(11)	9/2−				
		617.9	1.15	0.0	11/2−
854.90(12)	5/2+				
		827.2	2.89	27.7	3/2+
		639.5	0.08	215.2	1/2+
930.44(12)	3/2+				
		902.8	2.06	27.7	3/2+
		715.3	0.49	215.2	1/2+
936.55(11)	7/2−				
		936.5	1.66	0.0	11/2−
		318.6	0.02	617.9	9/2−
1059.54(14)	7/2+				
		1031.7	0.27	27.7	3/2+
1072.00(12)	3/2+				
		1044.3	1.16	27.7	3/2+
		856.8	1.07	215.2	1/2+
1187.53(12)	1/2+				
		1160.0	2.12	27.7	3/2+
		972.3	1.86	215.2	1/2+
		332.5	0.04	854.9	5/2+
		256.8	0.01	930.4	3/2+
1250.10(13)	7/2−				
		632.2	0.45	617.9	9/2−
1259.20(13)	5/2+				
		1231.5	1.38	27.7	3/2+
		1044.5	0.11	215.2	1/2+
		403.7	0.01	854.9	5/2+
1362.19(20)	7/2+				
		1334.7	0.24	27.7	3/2+
		506.9	0.03	854.9	5/2+
		431.9	0.01	930.4	3/2+
		302.3	0.00	1059.5	7/2+
		103.5	0.00	1259.2	5/2+
1538.75(13)	5/2+				
		1511.1	1.53	27.7	3/2+
		1323.9	0.03	215.2	1/2+
		683.9	0.16	854.9	5/2+
		608.4	0.03	930.4	3/2+
		602.2	0.02	936.5	7/2−
		479.2	0.02	1059.5	7/2+
		351.1	0.01	1187.5	1/2+
1599.12(12)	5/2−				
		981.3	0.33	617.9	9/2−
		744.3	0.09	854.9	5/2+
		662.6	0.12	936.5	7/2−
		539.5	0.00	1059.5	7/2+
		349.0	0.04	1250.1	7/2−
1683.57(14)	1/2+,3/2				
		1655.8	0.02	27.7	3/2+
		1468.3	0.07	215.2	1/2+
		828.9	0.14	854.9	5/2+
		753.3	0.05	930.4	3/2+
		611.5	0.08	1072.0	3/2+
1693.47(12)	5/2−				
		1075.5	0.15	617.9	9/2−
		763.1	0.01	930.4	3/2+
		756.8	0.15	936.5	7/2−
		633.7	0.01	1059.5	7/2+
		506.3	0.02	1187.5	1/2+
		443.2	0.02	1250.1	7/2−
		434.3	0.03	1259.2	5/2+
1746.63(24)	(7/2+)				
		891.7	0.03	854.9	5/2+
		816.3	0.01	930.4	3/2+
		487.4	0.01	1259.2	5/2+
1757.91(14)	1/2+				
		1542.7	0.30	215.2	1/2+
		904.5	0.09	854.9	5/2+
		827.6	0.33	930.4	3/2+
		685.9	0.02	1072.0	3/2+
1794.28(14)	(3/2−)				
		1579.1	0.25	215.2	1/2+
		857.7	0.19	936.5	7/2−
		722.2	0.06	1072.0	3/2+
		606.7	0.03	1187.5	1/2+
1796.42(13)	5/2+				
		1768.6	0.61	27.7	3/2+
		1581.5	0.20	215.2	1/2+
		859.8	0.07	936.5	7/2−
		608.9	0.03	1187.5	1/2+
1844.30(16)	11/2−,7/2−				
		1226.4	0.04	617.9	9/2−
		907.7	0.05	936.5	7/2−
		585.1	0.02	1259.2	5/2+
1874.41(14)	5/2+				
		1846.7	0.31	27.7	3/2+
		1019.9	0.04	854.9	5/2+
		943.7	0.02	930.4	3/2+
		802.2	0.02	1072.0	3/2+
		686.5	0.01	1187.5	1/2+
1884.09(14)	3/2−				
		1669.0	0.65	215.2	1/2+
		1029.2	0.14	854.9	5/2+
		953.6	0.01	930.4	3/2+
		947.5	0.03	936.5	7/2−
		812.0	0.01	1072.0	3/2+
		696.4	0.02	1187.5	1/2+
1901.83(25)	5/2−,7/2−				
		1283.9	0.03	617.9	9/2−
		651.8	0.02	1250.1	7/2−
		303.5	0.001	1599.1	5/2−
1938.21(15)	1/2+,3/2+				
		1911.2	0.11	27.7	3/2+
		1083.0	0.03	854.9	5/2+
		1007.7	0.04	930.4	3/2+
		866.1	0.02	1072.0	3/2+
		750.9	0.01	1187.5	1/2+
		678.4	0.01	1259.2	5/2+

TABLE V. (*Continued.*)

E_i(keV)	Spin	E_γ(keV)	I_γ(%)	E_f(keV)	Spin
1967.44(15)	1/2+,3/2,5/2+				
		1940.1	0.20	27.7	3/2+
		1752.9	0.07	215.2	1/2+
		1112.3	0.06	854.9	5/2+
		1036.9	0.06	930.4	3/2+
		780.4	0.01	1187.5	1/2+
		708.1	0.02	1259.2	5/2+
1984.22(16)	(7/2−)				
		1366.7	0.02	617.9	9/2−
		1129.5	0.04	854.9	5/2+
		1047.6	0.02	936.5	7/2−
		734.1	0.04	1250.1	7/2−

The fit of the spin distribution of the 35 low-lying levels within the spin range from 1/2 to 7/2 with the $f(J)$ function is shown in Fig. 13. The result of this fit is $\sigma = 3.4 \pm 0.6$. This value is slightly smaller than the value $\sigma = 3.97$ calculated from the systematics $\sigma = (0.98 \pm 0.23)A^{(0.29\pm0.06)}$ [42].

Negative parity states were observed mainly in the (d, p) reaction. The high sensitivity of this reaction enables us to see also states with more complicated structures. It is also important that the experimental range of excitation energies covers the whole distribution of the strengths of the $p_{1/2}$, $p_{3/2}$, $f_{5/2}$, and $f_{7/2}$ subshells (see Sec. IV B and Fig. 16). Therefore no spin is preferred by the reaction. Considering these conditions, the almost perfect fit in Fig. 13 should not be overestimated. Nevertheless, the resulting value of $\sigma = 3.75 \pm 0.24$ seems to be reasonable. It should be noted that to treat this value as the general spin cutoff parameter one has to accept other assumptions, namely parity symmetry, proton-neutron single-particle symmetry, as well as similar spin distribution for states with very complicated structures.

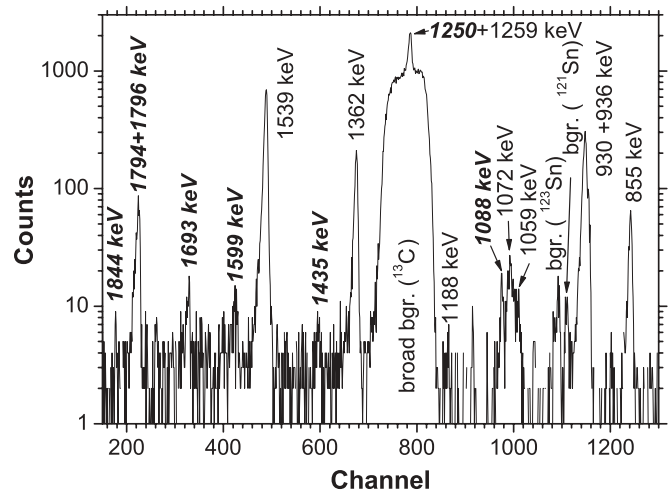

FIG. 8. The low-energy part of the proton spectrum from the reaction ^{124}Sn$(d, p)^{125}$Sn measured at beam energy $E_d =$ 22 MeV, scattering angle $\theta_{lab} = 20°$, and vector polarization $P = +70\%$. Newly established levels are labeled by a bold font.

IV. QUASIPARTICLE-PHONON MODEL

A. Description of QPM

Nuclear structure calculations of the properties of low-lying states in ^{125}Sn have been performed within the quasiparticle-phonon model (QPM). They are very similar in detail to the QPM calculations in odd-mass tellurium isotopes [5–7] and ^{113}Cd [51], published recently.

Briefly, we describe the ground and excited states of an odd-mass nucleus with total angular momentum J by a wave function which contains different [quasiparticle × N phonons] configurations (to be notated as [qp × Nph] with $N = 0$, 1, and 2):

$$\Psi^\nu(JM) = \left\{ C^\nu(J)\alpha^+_{JM} + \sum_{j\lambda i} S^\nu_{j\lambda i}(J)[\alpha^+_j Q^+_{\lambda i}]_{JM} + \sum_{j\beta_1\beta_2 l} \frac{D^\nu_{j\beta_1\beta_2}(J)[\alpha^+_j [Q^+_{\beta_1} Q^+_{\beta_2}]_l]_{JM}}{\sqrt{1+\delta_{\beta_1\beta_2}}} \right\} |^{124}\mathrm{Sn}\rangle_{\mathrm{g.s.}} \quad (5)$$

where α^+_j is a quasiparticle creation operator for an odd neutron on a mean-field level $j = |nlj\rangle$, Q^+_β is a phonon excitation of the core nucleus ^{124}Sn with the bosonic quantum numbers $\beta = |\lambda\mu i\rangle$ ($i = 1, 2$, etc., is an order number for each multipolarity λ), and $|^{124}\mathrm{Sn}\rangle_{\mathrm{g.s.}}$ is the ground-state wave function of the core. The mean field is described by the Woods-Saxon potential with parameters for $A = 121$ from Ref. [52]. Phonons are made up from proton and neutron two-quasiparticle configurations.

At the first stage, we have solved the quasiparticle RPA equations in ^{124}Sn and obtained the phonon basis for the natural parity states with the multipolarity λ from 2 to 8. Dipole excitations do not play an essential role at low excitation energies. The strength of the residual interaction has been adjusted to reproduce the experimental properties of the 2^+_1 and 3^-_1 states.

Then, the model Hamiltonian has been diagonalized on the set of states of Eq. (5) for different values of the total angular momentum J. The diagonalization yields eigenenergies of the states of Eq. (5) and coefficients C, S, and D. Index $\nu = 1, 2, \ldots$ is an order number of the state with the total angular momentum J.

All [qp × Nph] configurations allowed by spin and parity conservation are included in the wave function (5). To make numerical calculations possible, the basis has been truncated by accounting for only [qp × 1ph] configurations below 6.5 MeV and [qp × 2ph] configurations below 7.5 MeV. The calculations in the odd-mass ^{125}Sn nucleus have no free parameters. The matrix elements of the interaction between different configurations in the wave function (5) are calculated microscopically making use the model Hamiltonian and internal fermion structure of phonons. For more details on the QPM application to the description of odd-mass nuclei we refer to Ref. [53].

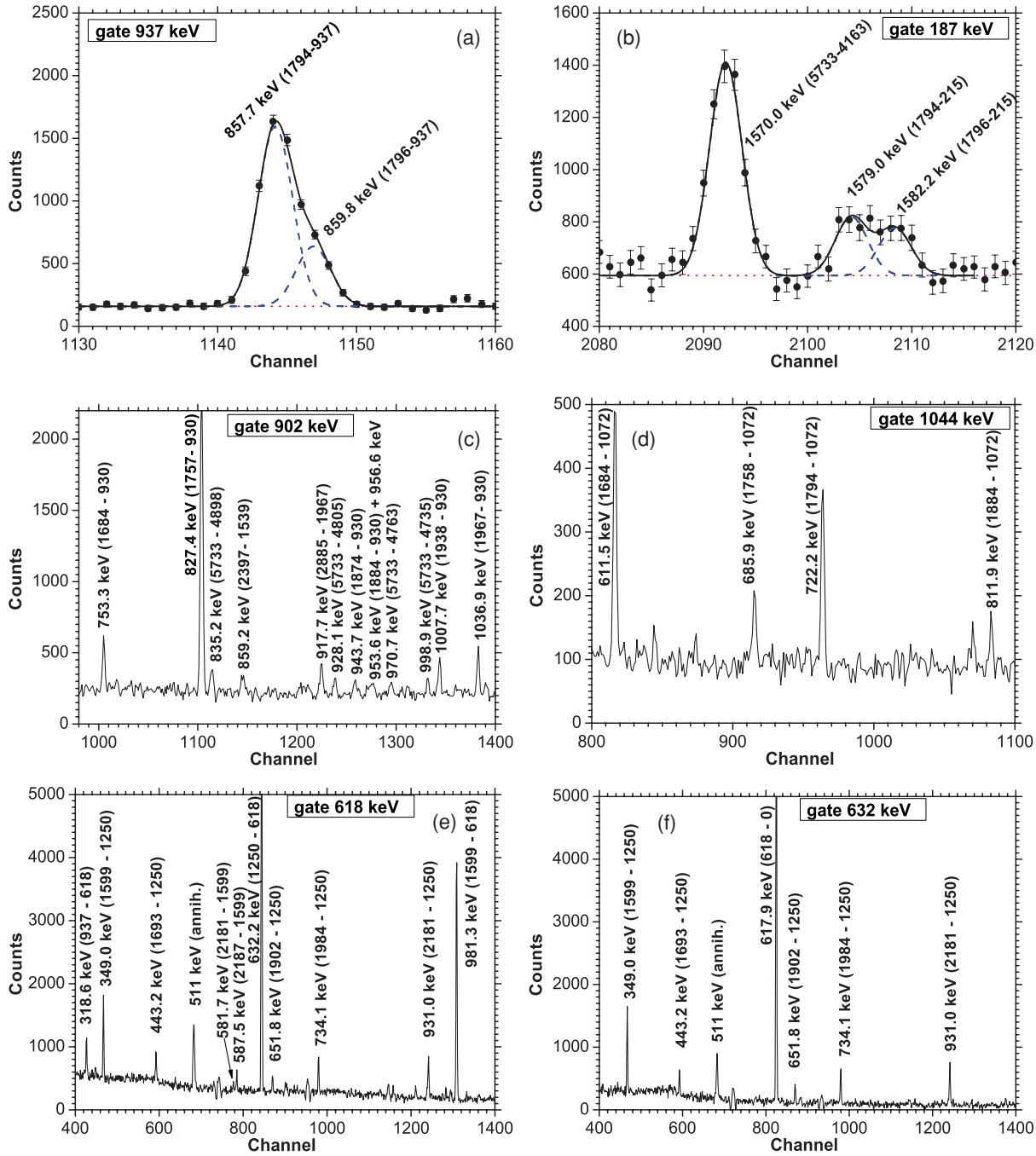

FIG. 9. (Color online) Parts of coincidence spectra relevant to newly established levels; see discussion in Sec. III B.

B. Comparison of experimental data with QPM calculations

The rich and different experimental data were compared with theoretical values from QPM calculations. This complex comparison allowed us to test the capabilities of the QPM for the theoretical calculation of various observables. From the other side, theoretical calculations can help us to understand the nuclear structure of the semi-magic ^{125}Sn isotope.

The mutual assignment of corresponding experimental and theoretical states is the first and most basic step of this comparison. To find this assignment we checked the excitation energies, the values of the (d,p) spectroscopic factors, and the branchings ratios. To obtain a realistic comparison of the branching ratios we corrected the QPM branchings for the experimental energies of the γ transitions. The result of the assignment procedure can be seen in Fig. 14. We obtained a firm assignment of theoretical states to experimentally observed levels up to an excitation energy of experimental levels of about 1.6 MeV. Below this excitation energy one can find an unambiguous assignment and the QPM calculation can reproduce all checked observables relatively well. A complementary comparison for the (d,p) spectroscopic

TABLE VI. The primary γ transitions from the ^{125}Sn(n,γ) reaction. γ energies E_γ are recoil corrected.

E_γ(keV)	I_γ(%)	E_f(keV)	Spin
4803.3	0.03	930.4	3/2+
4661.2	0.02	1072.0	3/2+
4545.9	0.04	1187.5	1/2+
3938.8	0.04	1794.3	(3/2−)
3849.4	0.15	1884.1	3/2−
3794.4	0.03	1938.2	1/2+,3/2+
3546.3	0.03	2186.7	(5/2+)
3385.7	0.11	2347.8	3/2−
3334.9	0.05	2397.6	1/2+,3/2,5/2+
3172.4	0.19	2561.3	3/2−
3151.0	0.09	2582.6	(3/2−)
2963.1	0.03	2770.5	1/2,3/2,5/2+
2848.1	0.18	2885.5	3/2−
2656.2	0.02	3077.4	1/2,3/2,5/2+
2569.7	0.20	3163.7	3/2−
2496.9	0.43	3236.7	3/2−
2397.3	9.68	3336.1	3/2−
2371.2	1.31	3362.3	3/2−
2324.7	27.95	3408.7	3/2−
2269.6	4.23	3463.7	3/2−
2257.3	1.13	3476.2	3/2−
2220.3	0.43	3513.4	1/2−
2199.8	2.73	3533.6	3/2−
2175.5	0.14	3558.1	3/2−
2151.9	0.15	3581.4	3/2−
2116.4	1.48	3617.1	3/2−
2031.1	0.09	3702.5	(3/2−)
1991.5	0.02	3742.2	3/2−
1944.2	0.11	3789.0	3/2−
1926.7	1.77	3806.8	3/2−
1904.5	1.13	3829.0	3/2−
1889.9	1.13	3843.6	3/2−
1872.4	1.85	3861.0	1/2−
1826.7	0.35	3906.8	1/2−
1782.6	0.48	3951.0	3/2−
1724.3	8.93	4009.1	1/2−
1710.4	8.67	4023.0	1/2−
1706.4	0.24	4026.9	1/2−
1683.8	0.68	4049.6	3/2−
1668.8	0.12	4064.9	1/2−,3/2−
1664.1	0.69	4069.4	3/2−
1641.7	0.90	4091.8	3/2−
1602.9	0.43	4130.6	3/2−
1583.2	0.27	4150.3	1/2−,3/2−
1578.8	0.21	4154.6	1/2−,3/2−
1570.0	1.55	4163.5	3/2−
1542.9	1.32	4190.7	3/2−
1538.1	0.31	4195.4	1/2−,3/2−
1523.7	0.15	4209.7	1/2−,3/2−
1463.6	0.40	4269.8	3/2−
1455.6	0.21	4278.0	1/2−
1447.4	0.89	4285.8	3/2−
1421.6	0.04	4311.8	1/2−,3/2−
1420.2	0.37	4313.3	3/2−
1411.1	0.35	4322.4	3/2−
1376.4	0.26	4357.0	(1/2−)
1349.7	0.34	4383.8	1/2−
1323.6	0.10	4410.0	3/2−
1321.1	0.33	4412.4	1/2−
1310.5	0.15	4423.0	3/2−
1301.0	0.46	4432.5	3/2−
1287.0	0.17	4446.5	3/2−
1282.4	0.16	4451.2	1/2−
1263.8	0.51	4469.3	3/2−
1236.7	0.69	4496.9	3/2−
1209.6	0.09	4523.4	1/2−,3/2−
1196.9	0.96	4536.6	1/2−
1192.8	0.12	4540.6	1/2−,3/2−
1174.0	0.36	4559.5	1/2−
1168.1	0.17	4565.0	1/2−,3/2−
1139.2	0.14	4594.4	1/2−,3/2−
1131.3	0.10	4602.6	1/2−,3/2−
1127.5	0.14	4606.1	1/2−,3/2−
1098.9	0.31	4634.2	1/2−,3/2−
1089.1	0.11	4644.3	1/2−,3/2−
1086.6	0.18	4646.8	1/2−,3/2−
1074.8	0.10	4658.7	1/2−,3/2−
1042.3	0.32	4691.3	1/2−,3/2−
1038.2	0.20	4695.3	1/2−,3/2−
1022.2	0.06	4711.1	1/2−,3/2−
1020.8	0.13	4712.8	1/2−,3/2−
1008.3	0.70	4725.1	1/2−
998.9	0.17	4734.6	3/2−
983.7	0.09	4749.7	1/2−,3/2−
970.7	0.12	4762.8	3/2−
957.9	0.13	4775.7	1/2−,3/2−
956.6	0.04	4777.0	1/2−,3/2−
928.1	0.20	4805.3	1/2−,3/2−
919.2	0.20	4814.5	3/2−
908.7	0.22	4824.7	3/2−
882.8	0.04	4849.3	1/2−,3/2−
877.5	0.07	4855.9	1/2−,3/2−
861.6	0.11	4871.5	1/2−,3/2−
835.5	0.17	4898.0	3/2−
827.1	0.20	4906.4	1/2−,3/2−
781.5	0.12	4952.0	1/2−,3/2−
774.2	0.08	4959.3	1/2−,3/2−
769.7	0.16	4963.7	1/2−,3/2−
760.9	0.06	4972.6	1/2−,3/2−
754.0	0.09	4979.5	3/2−
730.6	0.05	5002.5	1/2−,3/2−
700.6	0.30	5033.3	1/2−
696.3	0.14	5037.1	(3/2−)
685.5	0.13	5047.8	1/2−,3/2−
678.5	0.10	5054.9	1/2−,3/2−
668.8	0.07	5064.3	1/2−,3/2−
664.6	0.13	5069.5	1/2−,3/2−
650.4	0.31	5083.1	1/2−,3/2−
633.2	0.07	5100.3	1/2−,3/2−
580.2	0.06	5153.4	(1/2−)
565.1	0.05	5168.2	1/2−,3/2−
528.8	0.03	5204.6	(1/2−)
464.0	0.04	5269.5	1/2−,3/2−

TABLE VI. (*Continued.*)

E_γ(keV)	I_γ(%)	E_f(keV)	Spin
447.1	0.20	5286.3	1/2−,3/2−
433.9	0.02	5299.1	1/2−,3/2−
427.1	0.08	5306.4	1/2−,3/2−
416.6	0.04	5316.8	1/2−,3/2−
410.6	0.04	5322.7	1/2−,3/2−
396.5	0.04	5336.9	1/2−,3/2−

factors, the branching ratios, and the summed spectroscopic strength is given in Fig. 15, Table VIII, and Table IX, respectively.

Taking into account the fact that the QPM calculation does not use any free parameters, the description of the low-energy features of ^{125}Sn by this truly microscopical calculation can be considered as reliable. Despite this relative success there are some points which deserve some comments and explanations.

It can be seen from Fig. 14 that theoretical states are predicted systematically at higher excitation energies than corresponding experimental levels. This small but systematic disagreement can be explained by the truncation of the model basis to [qp × 1ph] and [qp × 2ph] configurations as described in the previous subsection. The effect of lowering QPM states by accounting [qp × 3ph] components is well described and discussed in the study of the soft nucleus ^{113}Cd [51]. The role of these [qp × 3ph] components and more complex configurations is much smaller for the semi-magic nucleus ^{125}Sn. Most of the physical observables can be well calculated with a relatively simple basis. Nevertheless, one of the consequences of the omission of more complex configurations in the QPM calculation for ^{125}Sn can be seen in Fig. 14. Due to the very schematic residual interaction the QPM energy spectrum for the states with the same main quasiparticle-phonon configuration is more degenerate than the experimental one. This effect is most pronounced for

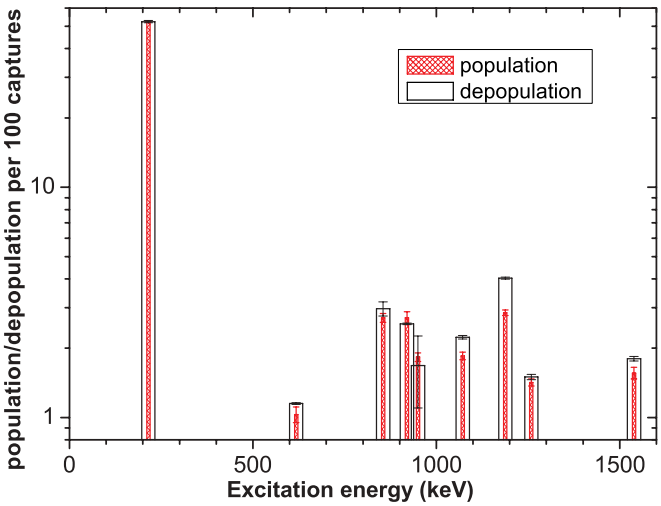

FIG. 10. (Color online) Population-depopulation balance for the low-lying levels. Only levels with a total depopulation higher than 1.0 per 100 neutron captures are depicted.

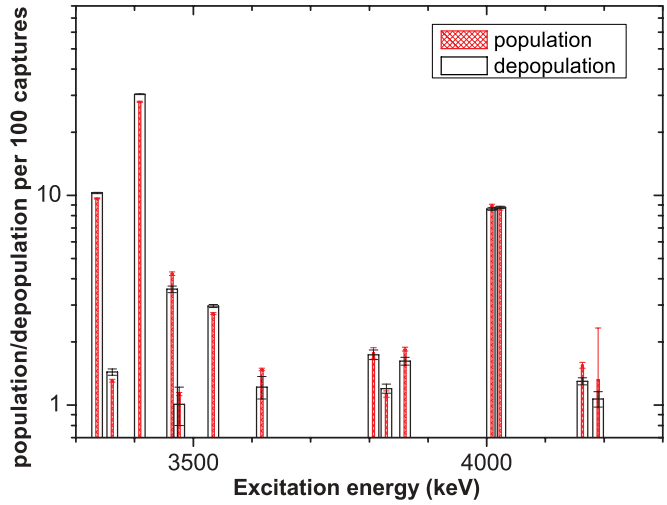

FIG. 11. (Color online) Population-depopulation balance for the levels populated by a primary transition. Only levels with a total depopulation higher than 1.0 per 100 neutron captures are depicted.

negative-parity states, which are dominated by $[1h_{11/2} \times 1\text{ph}]$ configurations.

The failure to reproduce the spectroscopic factor for the $5/2_2^+$ and $11/2_1^-$ states is another striking feature which emerged in the comparison (see Fig. 15). The QPM calculation gives a 40 times smaller spectroscopic factor for the $5/2_2^+$ state than we observed in the experiment. A similar failure was observed in the heavy-odd tellurium isotopes, ^{129}Te and ^{131}Te. In all these nuclei the theoretical models (besides QPM also IBFM for ^{129}Te and ^{131}Te) calculate a much smaller spectroscopic factor for these $5/2_2^+$ states. On the other hand, the theoretical models predict some concentration of a $2d_{5/2}$ strength at higher energies. It would indicate that the $2d_{5/2}$ single-particle energy is slightly overestimated in these calculations.

According to the QPM, the first $11/2^-$ state collects almost 100%, $[C^\nu(J)]^2 = 0.985$, of the $h_{11/2}$ strength in ^{125}Sn. A similar concentration of this strength was observed experimentally for ^{125}Sn as well as for the neighboring heavy odd-A tellurium isotopes. However, the QPM spectroscopic factor for forming the final state $11/2_1^-$ by a stripping reaction $S_{dp}(11/2_1^-) = u^2_{1h11/2} \times \left[C^1(11/2^-)\right]^2$ is almost three times higher than the observed experimental value. This difference is predominantly caused by the overestimated quasihole amplitude $u^2_{1h11/2}$, which characterizes the shell

TABLE VII. Systematics of the first $11/2^-$ state feeding in thermal neutron capture.

Final nucleus	Isomeric ratio $\sigma^{11/2}/\sigma^{\text{tot}}$	Reference
^{123}Te	0.17(3)	[3,41]
^{125}Te	0.17(2)	[4,41]
^{127}Te	0.16(2)	[5,41]
^{129}Te	0.11(1)	[6,41]
^{131}Te	0.054(2)	[7]
^{125}Sn	0.028(6)	this work

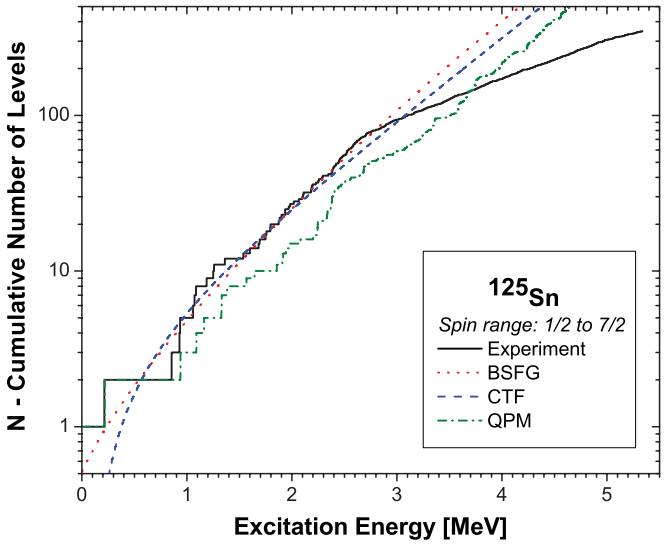

FIG. 12. (Color online) Comparison of the experimental cumulative number of levels with J from $1/2$ to $7/2$ with the model predictions of the BSFG, CTF, and QPM models. Note that the fit was also made to the s-wave neutron resonance spacing, which is not shown on the graphs.

occupancy/emptiness. This overestimation can be seen also in Table IX.

Besides the investigation in the low-energy part of the level scheme of ^{125}Sn, we looked at QPM predictions at higher excitation energies. Almost the whole range of distribution of spectroscopic strength was experimentally observed for four negative-parity subshells, $3p_{1/2}$, $3p_{3/2}$, $2f_{5/2}$, and $2f_{7/2}$. This experimental cumulative sum of spectroscopic factors is compared with the QPM prediction in Fig. 16. The position of the spectroscopic strength distributions, which is represented in Fig. 16 by a sharp rising, is reproduced by the QPM prediction relatively well. Only a small shift of the strength distribution can be detected for the the $3p_{1/2}$ and $1f_{5/2}$ subshells. It would indicate a small overestimation of the

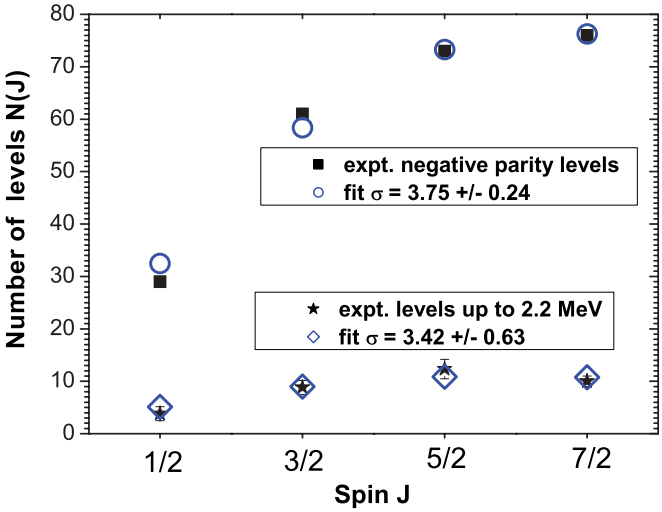

FIG. 13. (Color online) Fit of the spin cutoff parameter σ to the experimental data.

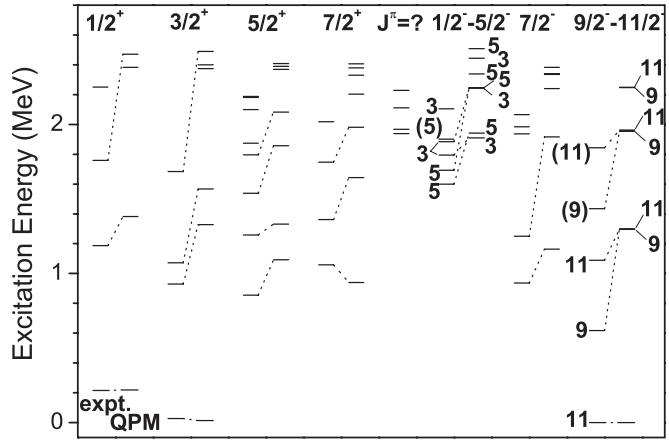

FIG. 14. The comparison of the experimental level energies with the QPM prediction in ^{125}Sn.

neutron quasiparticle energy in the Woods-Saxon potential. To test how QPM predicts the fragmentation of the spectroscopic strengths we looked at the number of experimentally observed and calculated levels below excitation energy $E < 6.3$ MeV and with a spectroscopic factor $S_{dp} \geqslant 10^{-3}$. Within these regions the experiment and the theory could give reasonably complete information. These numbers are compared in Fig. 17. For $3p_{1/2}$ and $1f_{5/2}$ the experiment gave significantly more states with a one-neutron transfer spectroscopic strength $S_{dp} \geqslant 10^{-3}$ than the QPM. In the theoretical calculation the strengths for these subshells are concentrated into the few strongest states. This lack of fragmentation is caused by the truncation of the basis. The $5/2^-$ and $1/2^-$ quasiparticle energies are higher than those of their upper spin shell partners. Therefore the fragmentation of the $1f_{5/2}$ and $3p_{1/2}$ strength was more affected by neglecting [qp $\times$ 1ph] configurations above 6.5 MeV than the fragmentation of the $1f_{7/2}$ and $3p_{3/2}$ strength.

In Sec. III D we investigated the level density of ^{125}Sn in the framework of the phenomenological CTF and BSFG models. These simple models are still very successful in

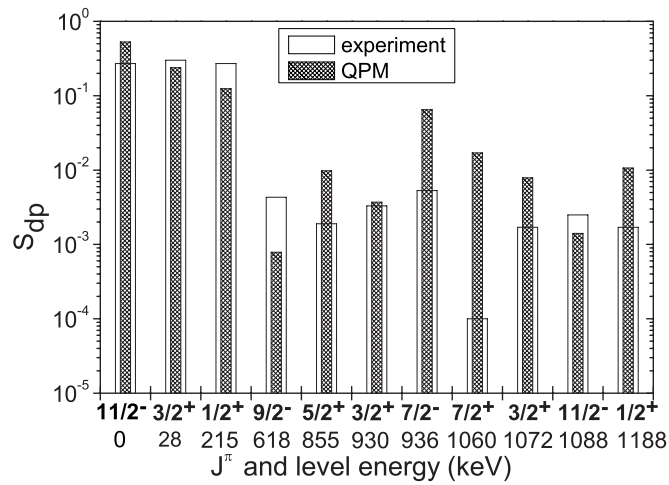

FIG. 15. The comparison between the experimental (d, p) spectroscopic factors and the QPM calculations.

TABLE VIII. Experimental and theoretical electromagnetic properties of ^{125}Sn states. Note that theoretical branchings were corrected for experimental transition energies.

E_i (MeV)	J_i	J_f	E_γ (MeV)	Expt.	QPM
		Positive parity states			
0.215	$1/2_1$	$3/2_1$	0.188	100	100
0.855	$5/2_1$	$3/2_1$	0.827	100	100
		$1/2_1$	0.639	2.8	0.5
0.930	$3/2_2$	$3/2_1$	0.903	100	100
		$1/2_1$	0.715	23.8	3.8
1.059	$7/2_1$	$3/2_1$	1.032	100	100
1.072	$3/2_3$	$3/2_1$	1.044	100	19.4
		$1/2_1$	0.857	92.2	100
1.188	$1/2_2$	$3/2_1$	1.169	100	92.9
		$1/2_1$	0.972	87.7	100
		$5/2_1$	0.332	2.1	
		$3/2_2$	0.257	0.2	
1.259	$5/2_2$	$3/2_1$	1.231	100	100
		$1/2_1$	1.044	8.0	4.7
		$5/2_1$	0.404	0.8	4.4
1.362	$7/2_2$	$3/2_1$	1.335	100	100
		$5/2_1$	0.507	11.7	
		$3/2_2$	0.432	3.7	
		$7/2_1$	0.302	0.8	0.2
		$5/2_2$	0.103	1.2	0.1
1.539	$5/2_3$	$3/2_1$	1.511	100	100
		$1/2_1$	1.324	1.8	13.1
		$5/2_1$	0.684	10.5	7.6
		$3/2_2$	0.608	2.2	3.8
		$7/2_1$	0.479	1.2	1.5
		$1/2_2$	0.351	0.6	
1.684	$(3/2_4)$	$3/2_1$	1.656	11.4	8.1
		$1/2_1$	1.468	52.9	23.5
		$5/2_1$	0.829	100	100
		$3/2_2$	0.753	32.9	7.2
		$3/2_3$	0.612	54.3	23.6
1.747	$(7/2_3)$	$5/2_1$	0.892	100	100
		$3/2_2$	0.816	28.6	14.8
		$5/2_2$	0.487	28.6	0.7
1.757	$1/2_3$	$1/2_1$	1.542	90.9	100
		$5/2_1$	0.905	27.5	4.5
		$3/2_2$	0.828	100	45.6
		$3/2_3$	0.686	63.6	19.2
1.796	$5/2_4$	$3/2_1$	1.769	100	100
		$1/2_1$	1.582	32.8	1.1
		$1/2_2$	0.609	5.4	
		Negative parity states			
0.618	$9/2_1$	$11/2_1$	0.618	100	100
0.936	$7/2_1$	$11/2_1$	0.937	100	100
		$9/2_1$	0.319	1.0	
1.250	$7/2_2$	$11/2_1$	1.250		100
		$9/2_1$	0.632	100	20.8
		$7/2_1$	0.314		0.79
1.599	$5/2_1$	$9/2_1$	0.981	100	8.3
		$7/2_1$	0.663	36.4	19.3
		$7/2_2$	0.349	11.8	100

TABLE IX. Sum rules for the (d,p) spectroscopic strength and single-particle neutron energies. Note that single-particle energies are presented relatively to $\varepsilon(1h_{11/2})$.

Shell	Expt.	QPM	ε (MeV)
$3s_{1/2}$	0.37	0.30	0.47
$2d_{3/2}$	1.11	1.08	0.15
$2d_{5/2}$	0.32	0.19	2.16
$1g_{7/2}$	0.21	0.37	1.60
$3p_{1/2}$	0.92	1.98	4.80
$3p_{3/2}$	1.84	3.96	4.21
$2f_{5/2}$	1.68	5.94	6.00
$2f_{7/2}$	3.28	7.84	3.13
$1h_{9/2}$	2.69	9.93	5.79
$1h_{11/2}$	2.19	6.42	0.00

comparison with attempts of microscopic calculations. The QPM prediction for the spin range from $1/2$ to $7/2$ is depicted in Fig. 12. The QPM data have the same trend as the CTF or BSFG models and up to 2.5 MeV as the experimental data. Considering the truncation of the basis in the QPM, which was described in Sec. IV A, also the quantitative comparison with the CTF and BSFG models seems to be promising, at least for this semi-magic nucleus ^{125}Sn.

C. Structure of low-lying states

The structure of the experimentally observed low-lying levels was investigated within the framework of the QPM. The satisfactory agreement between the experimental data and the QPM, which was presented in the previous section, can rationally justify performing this investigation.

1. Positive-parity states

The composition of the wave functions of the low-lying positive-parity states is given in Table X. The structure of these states is dominated by the $2d_{3/2}$, $3s_{1/2}$, $2d_{5/2}$, and $1g_{7/2}$ intrinsic single-particle configurations or by [qp $\times$ 1ph] configurations.

In ^{125}Sn, the $2d_{3/2}$ and $3s_{1/2}$ single-particle energies are far lower than the $2d_{5/2}$ and $1g_{7/2}$ energies. Using the QPM language we can disclose the family of levels built on pure $2d_{3/2}$ and $3s_{1/2}$ quasiparticle states at 28 and 215 keV, respectively. The levels at 930 keV (3/2), 1059 keV (7/2), 1187 keV (1/2), and 1259 keV (5/2) form a quadruplet of states with the $[2d_{3/2} \times 2_1^+]$ configuration. Tentatively, the $7/2^+$ and $5/2^+$ levels at 1746 and at 1796 keV, respectively, can be interpreted as the $[2d_{3/2} \times 4_1^+]$ doublet. Similarly, the $3/2^+$ level at 1072 keV is assigned to the $[3s_{1/2} \times 2_1^+]$ configuration. The $5/2^+$ component of the $[3s_{1/2} \times 2_1^+]$ doublet is not so evident. The QPM calculation shares the strength of this configuration almost evenly among the first three $5/2^+$ states. The γ-decay data also do not show a $5/2^+$ level with a strong decay branch to the $1/2_1^+$ level.

The QPM predicts minor contributions of $2d_{5/2}$ and $1g_{7/2}$ in the configurations of the low-lying levels. Neither the first

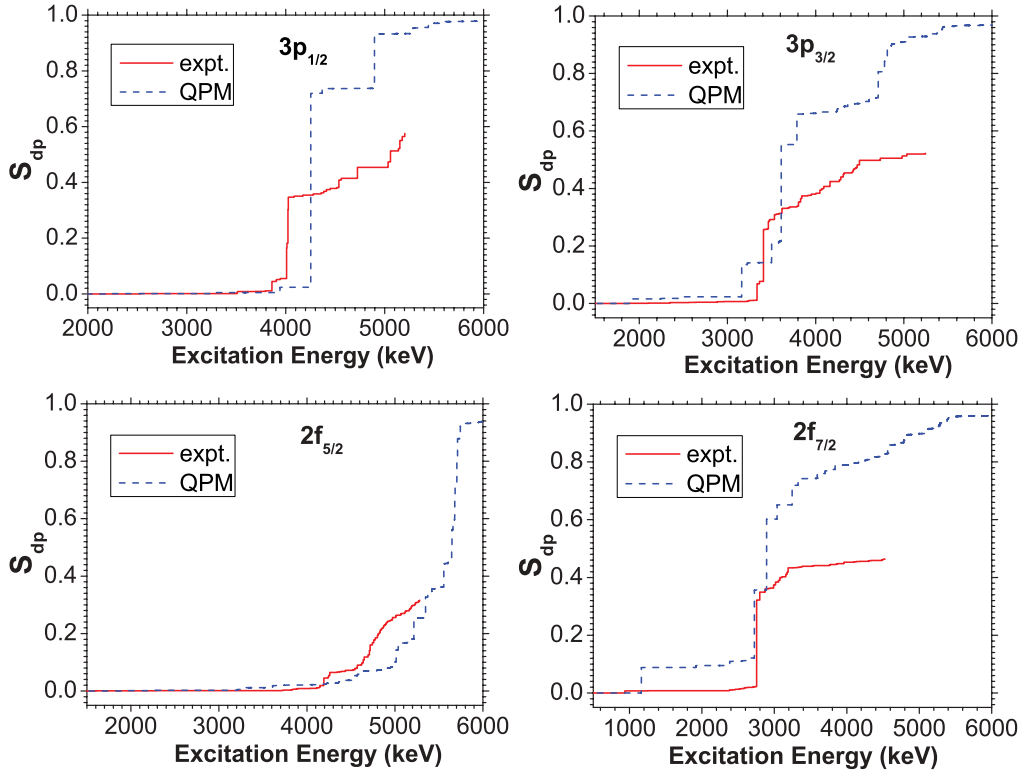

FIG. 16. (Color online) The experimental and QPM cumulative sums of spectroscopic factors S_{dp} for $3p_{1/2}$, $3p_{3/2}$, $2f_{5/2}$, and $2f_{7/2}$ orbitals in ^{125}Sn.

$5/2^+$ level nor the first $7/2^+$ level could be regarded as the states with a dominant single-particle configuration. However, it should be noted that the results on the spectroscopic strength suggest higher contributions of the $2d_{5/2}$ component especially in the structure of wave functions of levels around 1.3 MeV (see discussion in the previous Sec. IV B).

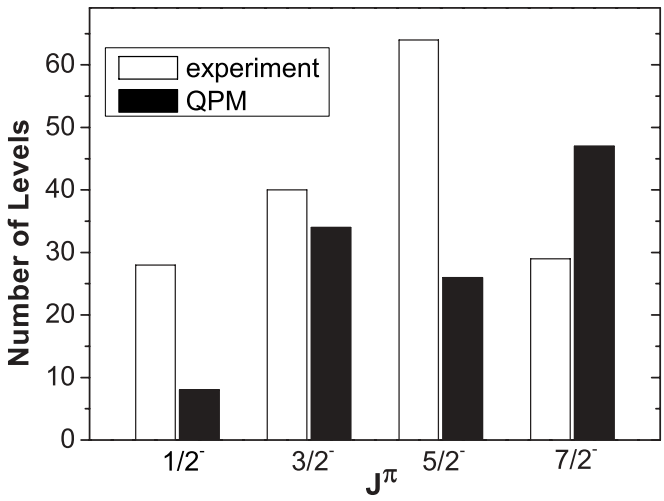

FIG. 17. The comparison of numbers of observed $1/2^-$, $3/2^-$, $5/2^-$, and $7/2^-$ levels with the QPM calculations. Both sets of numbers include states below excitation energy $E < 5.3$ MeV and with $S_{dp} \geqslant 10^{-3}$.

Table X foretells several states around 2.4 MeV with the coupling of the negative-parity single-particle state $1h_{11/2}$ with the high-spin phonon excitation 5^- or 7^-. Naturally, the very interesting question about the experimental observation and/or confirmation of these states arises. Addressing this challenging question we have found three hot candidates with this configuration. The levels at 1796, 2181, and 2186 keV possess a significant γ-decay branch to the $5/2^-$ and $7/2^-$ members of the $1h_{11/2}$ family of states.

2. *Negative-parity states*

The structure of the low-lying negative-parity states is strongly dominated by the $1h_{11/2}$ orbital (see Table XI). The single-particle energies for the other negative-parity orbitals, $2f_{7/2}$, $2f_{5/2}$, $3p_{3/2}$, and $3p_{1/2}$, are situated at much higher energies. The very small overlap between the distribution of strengths of these orbitals and the low-lying levels can be seen in our experimental results presented in Fig. 16. Therefore the low-lying negative-parity levels in ^{125}Sn are interpreted as almost pure members of the $1h_{11/2}$family of states. This family of states is formed by the coupling of the $1h_{11/2}$ neutron quasiparticle to 2^+, 4^+, and 6^+ phonons. The three levels at 618 keV ($9/2_1$), 936 keV ($7/2_1$), and 1087 keV ($11/2_2$) represent a triplet of states with the $[1h_{11/2} \times 2_1^+]$ configuration. The identification of the $[1h_{11/2} \times 4_1^+]$ "antialigned" quintuplet is more difficult and more tentative. Nevertheless, the $3/2^-$ level at 1794 keV, $5/2^-$ level at 1599 keV, $7/2^-$ level at 1250 keV,

TABLE X. Structure of wave function of positive-parity low-lying states in ^{125}Sn. Here j, N, L, and A^2 stand for the quantum numbers of the particles, the number of phonons, the phonon angular momentum, and the contribution to the wave function. Only main components of QPM wave function, Eq. (5), are listed.

I_i	E_x^{QPM}(MeV)	E_x^{expt}(MeV)	j	N	L	A^2 (%)
$1/2_1$	0.218	0.215	$3s_{1/2}$	0		83.1
			$2d_{3/2}$	1	2_1	10.1
$1/2_2$	1.383	1.187	$2d_{3/2}$	1	2_1	74.9
			$3s_{1/2}$	0		7.1
			$1g_{7/2}$	2	$4\,[2_1\times 2_1]$	5.1
$1/2_3$	2.382		$1h_{11/2}$	1	5_1	97.1
$1/2_4$	2.471	1.758	$2d_{3/2}$	1	2_2	74.9
			$2d_{3/2}$	2	$2\,[2_1\times 2_1]$	20.8
			$2d_{3/2}$	1	2_3	10.2
$3/2_1$	0.001	0.028	$2d_{3/2}$	0		88.3
$3/2_2$	1.375	0.930	$2d_{3/2}$	1	2_1	75.7
			$3s_{1/2}$	1	2_1	10.2
$3/2_3$	1.567	1.072	$3s_{1/2}$	1	2_1	67.2
			$2d_{3/2}$	1	2_1	9.8
			$2d_{3/2}$	2	$2\,[2_1\times 2_1]$	8.0
$3/2_4$	2.375		$1h_{11/2}$	1	5_1	97.5
$3/2_5$	2.400		$1h_{11/2}$	1	7_1	98.3
$3/2_6$	2.489	(1.684)	$2d_{3/2}$	1	2_2	44.4
			$2d_{3/2}$	2	$2\,[2_1\times 2_1]$	17.4
			$1g_{7/2}$	1	2_1	9.6
$5/2_1$	1.092	0.855	$2d_{5/2}$	0		30.6
			$3s_{1/2}$	1	2_1	26.5
			$2d_{3/2}$	1	2_1	25.0
$5/2_2$	1.332	1.259	$2d_{3/2}$	1	2_1	59.8
			$3s_{1/2}$	1	2_1	21.1
			$2d_{3/2}$	2	$4\,[2_1\times 2_1]$	6.5
$5/2_3$	1.857	1.539	$3s_{1/2}$	1	2_1	31.4
			$2d_{3/2}$	1	4_1	24.1
			$2d_{5/2}$	0		17.9
$5/2_4$	2.080	1.796	$2d_{3/2}$	1	4_1	57.8
			$2d_{5/2}$	0		13.3
$5/2_5$	2.369		$1h_{11/2}$	1	5_1	30.2
			$1g_{7/2}$	1	2_1	17.1
			$2d_{3/2}$	1	2_1	13.3
$5/2_6$	2.389		$1h_{11/2}$	1	5_1	42.5
			$1h_{11/2}$	1	7_1	39.2
$7/2_1$	0.940	1.059	$2d_{3/2}$	1	2_1	50.0
			$1g_{7/2}$	0		37.7
$7/2_2$	1.643	1.362	$2d_{3/2}$	1	2_1	37.0
			$1g_{7/2}$	0		35.9
			$1g_{7/2}$	1	2_1	8.7
			$2d_{3/2}$	1	4_1	5.2
$7/2_3$	1.981	1.746	$2d_{3/2}$	1	4_1	79.6
$7/2_4$	2.202		$3s_{1/2}$	1	4_1	72.0
$7/2_5$	2.331		$2d_{3/2}$	1	2_2	13.8
			$1h_{11/2}$	1	5_1	11.3
			$1g_{7/2}$	1	2_1	10.1
			$3s_{1/2}$	1	4_1	7.5
			$1g_{7/2}$	0		5.2
$7/2_6$	2.380		$1h_{11/2}$	1	5_1	75.0
			$1h_{11/2}$	1	7_1	16.3
$7/2_7$	2.406		$1h_{11/2}$	1	7_1	79.0
			$1h_{11/2}$	1	5_1	10.8

TABLE XI. Structure of wave function of negative-parity low-lying states in ^{125}Sn. See caption to Table X.

I_i	E_x^{QPM}(MeV)	$E_x^{\mathrm{expt.}}$(MeV)	j	N	L	A^2 (%)
$11/2_1$	0.000	0.000	$1h_{11/2}$	0		98.5
$11/2_2$	1.298	1.087	$1h_{11/2}$	1	2_1	97.0
$11/2_3$	1.962	(1.843)	$1h_{11/2}$	1	4_1	91.6
			$1h_{11/2}$	2	$4\,[2_1\times 2_1]$	7.3
$11/2_4$	2.249		$1h_{11/2}$	1	6_1	98.9
$9/2_1$	1.297	0.618	$1h_{11/2}$	1	2_1	97.4
$9/2_2$	1.954	(1.435)	$1h_{11/2}$	1	4_1	90.6
			$1h_{11/2}$	2	$4\,[2_1\times 2_1]$	7.9
$9/2_3$	2.247		$1h_{11/2}$	1	6_1	98.6
$7/2_1$	1.164	0.936	$1h_{11/2}$	1	2_1	89.1
			$2f_{7/2}$	0		6.6
$7/2_2$	1.917	1.250	$1h_{11/2}$	1	4_1	89.1
			$1h_{11/2}$	2	$4\,[2_1\times 2_1]$	8.6
$7/2_3$	2.241		$1h_{11/2}$	1	6_1	96.8
$7/2_4$	2.336		$1h_{11/2}$	2	$2\,[2_1\times 2_1]$	50.4
			$1h_{11/2}$	1	2_2	30.7
			$1h_{11/2}$	1	2_3	9.6
$7/2_5$	2.340		$1h_{11/2}$	1	8_1	98.6
$7/2_6$	2.383		$2d_{3/2}$	1	5_1	87.0
$5/2_1$	1.943	1.599	$1h_{11/2}$	1	4_1	87.7
			$1h_{11/2}$	2	$4\,[2_1\times 2_1]$	10.2
$5/2_2$	2.245	1.693	$1h_{11/2}$	1	6_1	98.6
$5/2_3$	2.339		$1h_{11/2}$	1	8_1	99.1
$5/2_4$	2.508		$1h_{11/2}$	2	$4\,[2_1\times 2_1]$	76.7
			$1h_{11/2}$	1	4_1	11.0
			$2f_{7/2}$	1	2_1	6.8
$3/2_1$	1.910	1.794	$1h_{11/2}$	1	4_1	82.5
			$1h_{11/2}$	2	$4\,[2_1\times 2_1]$	12.7
$3/2_2$	2.245	1.884	$1h_{11/2}$	1	6_1	98.2
$3/2_3$	2.443		$1h_{11/2}$	2	$4\,[2_1\times 2_1]$	68.8
			$1h_{11/2}$	1	4_1	15.4
			$2f_{7/2}$	1	2_1	10.0
$1/2_1$	2.245		$1h_{11/2}$	1	6_1	98.6

$(9/2^-)$ level at 1435 keV, and $(11/2^-)$ level at 1843 keV could constitute this quintuplet.

V. DIRECT NEUTRON CAPTURE MECHANISM

Regarding the lack of resonances close to the neutron binding energy, one could assume a stronger role of the direct capture mechanism in the ^{124}Sn$(n,\gamma)^{125}$Sn reaction. The investigation of the role of this mechanism in this reaction is one of the main goals of this paper. The evidence for the presence of this mechanism is the correlation between the spectroscopic strength in the one-neutron transfer reaction and the intensities of the primary transitions in the (n_{th},γ) reaction. Our (d,p) and (n_{th},γ) experiments give the excellent possibility to observe such correlations. For the detailed study of the role of the direct capture mechanism we used the old, but very successful, theory by Lane and Lynn [54] and the

formula for an even-even target [10]:

$$\sigma_{\gamma f}(\text{channel}) = \sigma_{\gamma f}(\text{hard sphere})\left[1+\frac{R-a_{\text{coh}}}{R}Y_f\frac{Y_f+2}{Y_f+3}\right]^2, \quad (6)$$

where

$$\sigma_{\gamma f}(\text{hard sphere}) = \frac{0.062}{R\sqrt{E_n}}\left[\frac{Z}{A}\right]\frac{2J_f+1}{6(2J_t+1)}S_{dp}Y_f^2\left[\frac{Y_f+3}{Y_f+1}\right]^2 \quad (7)$$

and

$$Y_f^2 = \frac{2mE_\gamma R^2}{\hbar^2}. \quad (8)$$

Z is the proton number, A is the atomic number, R is the interaction radius (usually taken in the form $1.35\times A^{1/3}$ fm), a_{coh} is the coherent scattering length, J_f is the total spin of final state, J_t is the spin of the target, S_{dp} is the (d,p) spectroscopic factor, E_γ is the energy of the primary γ transition, and E_n is the incident neutron energy (0.0253 eV for 2200 m/s neutrons).

For ^{125}Sn we found 55 states which were fed by the primary transitions in the (n_{th},γ) reaction and were assigned with an $l=1$ transfer in the (d,p) reaction. This large data set enables us to compare in detail the measured partial cross sections from the (n_{th},γ) reaction with the theoretical predictions of direct capture within the framework of the Lane-Lynn theory. The experimental partial cross sections were calculated from the absolute γ intensities using the total cross section 134 mb [10]. The theoretical values were calculated according to Eq. (6). The comparison of the results is depicted in Fig. 18. One can see the high correlation between the experimental and theoretical values. This correlation is well documented by the high value of the correlation coefficient, $\rho = 0.987$. Besides several very weak transitions there is one point which does not follow the general trend in Fig. 18. This point corresponds to the state at 1706 keV. The vicinity of the huge peak at 1710 keV in the proton spectra is probably responsible for this disagreement. Nevertheless, even without the primary intensity for this state, the points in Fig. 18 represent 86.4% of the total primary intensity. One can conclude that the thermal neutron capture on the ^{124}Sn isotope is dominated by the direct mechanism.

While there is no doubt about the correlation between the theoretical and experimental cross sections the disagreement between absolute values can be seen. The calculated values are almost two times smaller than the experimental values. The reason for this disagreement is not fully clear. In principle, there are three experimental quantities which could cause this difference, namely the absolute γ intensity of the primary transitions, the total thermal neutron capture cross section, and the spectroscopic factors S_{dp}.

We can exclude the possible systematic error caused by the γ intensity. The relative intensities were normalized via the β decay and independently checked by means of the total ground-state population. The experimental sum of primary-transition intensities, which amounts to 96.1γ per 100 thermal neutron captures, also confirms the absolute γ intensities.

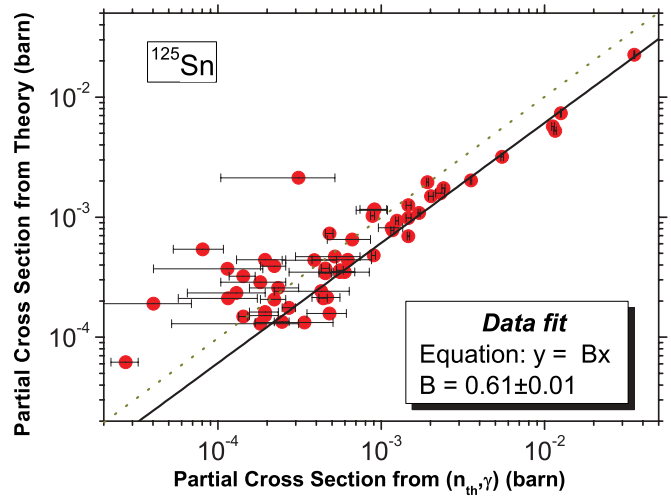

FIG. 18. (Color online) The comparison of the experimental partial cross section from the (n_{th},γ) with theoretical prediction from the Lane-Lynn model of direct capture. The solid line represents the linear fit of the data.

The other experimental quantity needed for the calculation of the partial cross section is the thermal neutron capture cross section for the neutron velocity $v = 2200$ m/s. The compiled value of this cross section, $\sigma^0 = (0.134 \pm 0.005)$ b, given in Ref. [10] is based on the work of Ref. [55]. This value is in good agreement with the previous measurements [56,57], $\sigma^0 = (0.125 \pm 0.018)$ b and $\sigma^0 = (0.15 \pm 0.03)$ b, respectively, as well as with the recommended value for ^{125}Sn^m in the work by Moens *et al.* [58], $\sigma^0 = 0.13$ b. Thus it is improbable that this quantity would be responsible for the systematic difference between the experimental partial cross sections and the calculated values according to Eq. (6).

Excluding the absolute intensities and the thermal neutron capture cross section as the source of the systematic disagreement we turn our attention to the values of the spectroscopic factors S_{dp}. Generally, the systematic uncertainty of these values due to the parameters of the optical model in DWBA is considered to be around 30%. A short discussion of these uncertainties was done above in Sec. II B3. The small room for a systematic increase of the S_{dp} factors for the $3p_{3/2}$ and $3p_{1/2}$ subshells can be found out in the sum of the spectroscopic factors (see Fig. 16). Thus the spectroscopic factors seem to be presumably responsible for the fitted average ratio between the experimental partial cross sections from the (n,γ) reaction and the calculated values, which is about 1.8.

VI. CONCLUSIONS

The combination of the experimental (d,p) and (n,γ) data in the present work yields a large amount of experimental information on ^{125}Sn. Some of these results are mutually interconnected. In this sense, this detailed study provides a consistent survey of the semi-magic nucleus ^{125}Sn.

The level scheme in this work consists of about 400 levels and about 750 placed γ transitions. This level scheme can be considered to be essentially complete in the spin range

below 7/2 up to 1.9 MeV of excitation energy, including level energies, spin-parity assignments, γ decay patterns, and in most cases also spectroscopic factors. This level scheme was interpreted in terms of the QPM.

Besides the study of the nuclear properties of the low-lying levels the extensive experimental data brought the unique collection of $1/2^-$, $3/2^-$, $5/2^-$, and $7/2^-$ states. This collection enables us to investigate the fragmentation of $3p_{1/2}$, $3p_{3/2}$, $2f_{5/2}$, and $2f_{7/2}$ strength. The experimental distributions were compared with QPM predictions.

More than 50 states fed by a primary transition give excellent opportunity to study the role of the direct mechanism in the thermal neutron capture of ^{124}Sn. The dominant role of direct mechanism is apparent from our results. Taking into account the completeness of the depopulation scheme of the capture state we can conclude that this mechanism is responsible for more than 95% of the total primary-transition intensity.

Using the experimental data from this work, we determined new and more precise values for some important nuclear quantities, such as the isomeric ratio, the neutron binding energy, and the parameters of the phenomenological level-density models.

ACKNOWLEDGMENTS

The work was supported by the Institute Research Plan AVOZ10480505, by the Grant Agency of the Czech Republic (Grant No. 202/03/0891), by the Ministry of Education, Youth, Sports of the Czech Republic (Grant No. 2672244501), by funds of the Munich Maier Leibnitz Laboratory, and by the Deutsche Forschungsgemeinschaft (Grant No. IIC4 Gr 894/2-3). V.Yu.P. acknowledges support by the DFG under Contract No. SFB 634.

[1] D. Bucurescu, T. von Egidy, H.-F. Wirth, N. Mărginean, U. Köster, G. Graw, A. Metz, R. Hertenberger, and Y. Eisermann, Nucl. Phys. A **674**, 11 (2000).
[2] D. Bucurescu, T. von Egidy, H.-F. Wirth, N. Mărginean, W. Schauer, I. Tomandl, G. Graw, A. Metz, R. Hertenberger, and Y. Eisermann, Nucl. Phys. A **672**, 21 (2000).
[3] V. Bondarenko, T. von Egidy, J. Honzátko, I. Tomandl, D. Bucurescu, N. Mărginean, J. Ott, W. Schauer, H.-F. Wirth, and C. Doll, Nucl. Phys. A **673**, 85 (2000).
[4] J. Honzátko, I. Tomandl, V. Bondarenko, D. Bucurescu, T. von Egidy, W. Schauer, H.-F. Wirth, C. Doll, A. Gollwitzer, G. Graw, R. Hertenberger, and B. Valnion, Nucl. Phys. A **645**, 331 (1999).
[5] J. Honzátko, V. Bondarenko, I. Tomandl, T. von Egidy, H.-F. Wirth, D. Bucurescu, V. Yu. Ponomarev, N. Mărginean, R. Hertenberger, Y. Eisermann, G. Graw, and L. Rubáček, Nucl. Phys. A **756**, 249 (2005).
[6] H.-F. Wirth, T. von Egidy, I. Tomandl, J. Honzátko, D. Bucurescu, N. Mărginean, V. Yu. Ponomarev, R. Hertenberger, Y. Eisermann, and G. Graw, Nucl. Phys. A **716**, 3 (2003).
[7] I. Tomandl, T. von Egidy, J. Honzátko, V. Bondarenko, H.-F. Wirth, D. Bucurescu, V. Yu. Ponomarev, G. Graw, R. Hertenberger, Y. Eisermann, and S. Raman, Nucl. Phys. A **717**, 149 (2003).
[8] I. F. Barchuk, V. I. Golyshkin, E. N. Gorban, and A. F. Ogorodnik, Izv. Akad. Nauk SSSR, Ser. Fiz. **45**, 727 (1981).
[9] C. R. Bingham and D. L. Hills, Phys. Rev. C **8**, 729 (1973).
[10] S. F. Mughabhab, M. Divadeenam, and N. E. Holden, *Neutron Cross Sections* (Academic, New York, 1981), Vol. 1.
[11] J. Honzátko, K. Konečný, I. Tomandl, J. Vacik, F. Bečvář, and P. Cejnar, Nucl. Instrum. Methods Phys. Res., Sect. A **376**, 434 (1996).
[12] M. Löffler, H. J. Scheerer, and H. Vonach, Nucl. Instrum. Methods **111**, 1 (1973).
[13] J. Katakura, Nucl. Data Sheets **86**, 955 (1999).
[14] R. F. Carlton, S. Raman, and G. G. Slaughter, Phys. Rev. C **15**, 883 (1977).
[15] C. P. Massolo, S. Fortier, S. Gales, F. Azaiez, E. Gerlic, J. Guillot, E. Hourani, H. Langevin-Joliot, J. M. Maison, J. P. Schapira, and G. M. Crawley, Phys. Rev. C **43**, 1687 (1991).
[16] G. C. Madueme, L. O. Edvardson, and L. Westerberg, Phys. Scr. **13**, 17 (1976).
[17] B. Fogelberg, L.-E. De Geer, K. Fransson, and M. af Ugglas, Z. Phys. A **276**, 381 (1976).
[18] Evaluated Nuclear Structure Data File (ENSDF), [http://ie.lbl.gov/ensdf/].
[19] C. van der Leun, P. de Wilt, and C. Alderliesten, in *Proceedings of the 4th Capture Gamma-ray Spectroscopy and Related Topics*, edited by T. von Egidy (Institute of Physics, Bristol, 1981), Vol. 62, p. 548.
[20] B. Krusche, K. P. Lieb, H. Daniel, T. von Egidy, G. Barreau, H. G. Börner, R. Brissot, C. Hofmeyr, and R. Rauscher, Nucl. Phys. A **386**, 245 (1982).
[21] R. Vennink, J. Kopecký, P. M. Endt, and P. W. M. Glaudemans, Nucl. Phys. A **344**, 421 (1980).
[22] R. G. Helmer, P. H. M. Van Assche, and C. van der Leun, At. Data Nucl. Data Tables **24**, 39 (1979).
[23] G. L. Molnar, Z. Revay, and T. Belgya, in *Proceedings of the 5th Topical Meeting on Industrial Radiation and Radioisotope Measurement Applications (IRRMA-V), Bologna, Italy, 2002* [Nucl. Instr. Meth. B **213**, 32 (2004)].
[24] *Table of Isotopes*, edited by R. B. Firestone, S. Y. F. Chu, and C. M. Baglin (Wiley, New York, 1999).
[25] Experimental Nuclear Reaction Data (EXFOR DB): [http://www-nds.iaea.org/exfor/exfor00.htm], entry number 31604.
[26] R. Hertenberger, A. Metz, Y. Eisermann, K. El Albiary, A. Ludewig, C. Pertl, S. Trieb, H.-F. Wirth, P. Schiemenz, and G. Graw, Nucl. Instrum. Methods Phys. Res., Sect. A **536**, 266 (2005).
[27] H.-F. Wirth, H. Angerer, T. von Egidy, Y. Eisermann, G. Graw, and R. Hertenberger, *New Q3D Focal Plane Detector with Cathode-Strip Readout became Operational*, Beschleunigerlaboratorium der Universität and der Technische Universität München Jahresbericht 2000, p. 71; H.-F. Wirth, Ph.D. thesis, Technical University Munich, Munich, 2001.
[28] F. Riess, GASPAN at the UNIX computers, Beschleunigerlaboratorium der Universität und der Technischen Universität München, Jahresbericht, 1991, p. 168.

[29] Experimental Nuclear Reaction Data (EXFOR DB): [http://www-nds.iaea.org/exfor/exfor00.htm], entry number D0457.
[30] P. D. Kunz, Computer Code CHUCK3, University of Colorado, [http://spot.colorado.edu/∼kunz].
[31] A. Strömich, B. Steinmetz, R. Bangert, B. Gonsior, M. Roth, and P. von Brentano, Phys. Rev. C **16**, 2193 (1977).
[32] S. Raman, C. W. Nestor, and P. Tikkanen, At. Data Nucl. Data Tables **78**, 1 (2001); [http://www.nndc.bnl.gov/be2/].
[33] A. M. Mukhamedzhanov, H. L. Clark, C. A. Gagliardi, Y.-W. Lui, L. Trache, R. E. Tribble, H. M. Xu, X. G. Zhou, V. Burjan, J. Cejpek, V. Kroha, and F. Carstoiu, Phys. Rev. C **56**, 1302 (1997).
[34] A. M. Mukhamedzhanov and F. M. Nunes, Phys. Rev. C **72**, 017602 (2005).
[35] L. J. B. Goldfarb and E. Parry, Nucl. Phys. A **116**, 309 (1968).
[36] W. R. Hering, H. Becker, C. A. Widner, and W. J. Thompson, Nucl. Phys. A **151**, 33 (1970).
[37] E. J. Schneid, A. Prakash, and B. L. Cohen, Phys. Rev. **156**, 1316 (1967).
[38] K. L. Jones, R. L. Kozub, C. Baktash, D. W. Bardayan, J. C. Blackmon, W. N. Catford, J. A. Cizewski, R. P. Fitzgerald, M. S. Johnson, R. J. Livesay, Z. Ma, C. D. Nesaraja, D. Shapira, M. S. Smith, J. S. Thomas, and D. W. Visser, Phys. Rev. C **70**, 067602 (2004).
[39] K. Schreckenbach, Program LEVFIT, ILL, Grenoble, 1975.
[40] G. Audi, A. H. Wapstra, and C. Thibault, Nucl. Phys. A **729**, 337 (2003).
[41] I. Tomandl, J. Honzátko, T. von Egidy, H.-F. Wirth, T. Belgya, M. Lakatos, L. Szentmiklósi, Zs. Revay, G. L. Molnar, R. B. Firestone, and V. Bondarenko, Phys. Rev. C **68**, 067602 (2003).
[42] T. von Egidy, H. H. Schmidt, and A. N. Bekhami, Nucl. Phys. A **481**, 189 (1988).
[43] A. Gilbert and A. G. W. Cameron, Can. J. Phys. **43**, 1446 (1965).
[44] T. von Egidy and D. Bucurescu, Phys. Rev. C **72**, 044311 (2005); D. Bucurescu and T. von Egidy, *ibid.* **72**, 067304 (2005); T. von Egidy and D. Bucurescu, *ibid.* **73**, 049901(E) (2006).
[45] H. Zhongfu, H. Ping, S. Zongdi, and Z. Chunmei, Chin. J. Nucl. Phys. **13**, 147 (1991).
[46] G. Reffo, Report No. IAEA-TECDOC-1034, International Atomic Energy Agency, Vienna, 1998, p. 25; RIPL-2 database [http://www.nds.iaea.org].
[47] R. Fischer, G. Traxler, M. Uhl, and H. Vonach, Phys. Rev. C **30**, 72 (1984).
[48] C. C. Lu, C. L. Vaz, and J. R. Huizenga, Nucl. Phys. A **197**, 321 (1972).
[49] P. Hill, P. Sperr, M. Hille, K. Rudolph, W. Assmann, and D. Evers, Nucl. Phys. A **232**, 157 (1974).
[50] S. M. Grimes, J. D. Anderson, J. W. McClure, B. A. Pohl, and C. Wong, Phys. Rev. C **10**, 2373 (1974).
[51] D. Bucurescu, Y. Eisermann, G. Graw, R. Hertenberger, H.-F. Wirth, and V. Yu. Ponomarev, Nucl. Phys. A **756**, 54 (2005).
[52] C. A. Bertulani and V. Yu. Ponomarev, Phys. Rep. **321**, 139 (1999).
[53] S. Galès, Ch. Stoyanov, and A. I. Vdovin, Phys. Rep. **166**, 125 (1988).
[54] A. M. Lane and J. E. Lynn, Nucl. Phys. **17**, 563 (1960); **17**, 586 (1960).
[55] G. Gleason, Radiochem. Radioanal. Lett. **26**, 39 (1976).
[56] S. K. Mangal and P. S. Gill, Nucl. Phys. **41**, 372 (1963).
[57] D. J. Hughes, R. C. Garth, and J. S. Levin, Phys. Rev. **91**, 1423 (1953).
[58] L. Moens, A. Simonits, F. de Corte, and J. Hoste, J. Radioanal. Chem. **54**, 377 (1979).